Czech Technical University in Prague
Faculty of Electrical Engineering

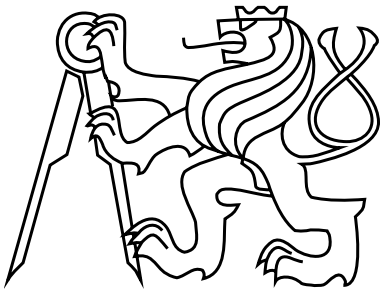

DIPLOMA THESIS

Modeling and state estimation of automotive SCR catalyst

Jiří Figura

Praha, 2016

Supervisor: Ing. Jaroslav Pekař, Ph.D.

Czech Technical University in Prague
Faculty of Electrical Engineering

Department of Control Engineering

DIPLOMA THESIS ASSIGNMENT

Student: **Bc. Jiří Figura**

Study programme: Cybernetics and Robotics
Specialisation: Systems and Control

Title of Diploma Thesis: **Modeling and state estimation of automotive SCR catalyst**

Guidelines:

1. Get introduced to automotive SCR and combined SCR/DPF systems
2. Provide an overview of the state-of-the-art in SCR state estimation and SCR modeling
3. Develop a model of automotive SCR catalyst for online estimation
4. Design an SCR estimator/observer of NH3 storage and analyze its performance

Bibliography/Sources:

[1] I. Nova and E. Tronconi, Eds., Urea-SCR Technology for deNOx After Treatment of Diesel Exhausts. New York, NY: Springer New York, 2014
[2] C. Ericson, B. Westerberg, and I. Odenbrand, A state-space simplified SCR catalyst model for real time applications, SAE Technical Paper, 2008
[3] H. S. Surenahalli, G. Parker, and J. H. Johnson, Extended Kalman Filter Estimator for NH3 Storage, NO, NO2 and NH3 Estimation in a SCR, SAE International, Warrendale, PA, 2013-01-1581, Apr. 2013
[4] H. Zhang, J. Wang, and Y.-Y. Wang, Robust Filtering for Ammonia Coverage Estimation in Diesel Engine Selective Catalytic Reduction Systems, Journal of Dynamic Systems, Measurement, and Control, vol. 135, no. 6, pp. 064504-064504, Aug. 2013

Diploma Thesis Supervisor: Ing. Jaroslav Pekař, Ph.D.

Valid until the summer semester 2016/2017

L.S.

prof. Ing. Michael Šebek, DrSc.
Head of Department

prof. Ing. Pavel Ripka, CSc.
Dean

Prague, October 15, 2015

Acknowledgments

I would like to thank Jaroslav Pekař, Ondřej Šantin and all the guys in Honeywell Automotive Software for their advice and assistance.

Declaration

Prohlašuji, že jsem předloženou práci vypracoval samostatně a že jsem uvedl veškeré použité informační zdroje v souladu s Metodickým pokynem o dodržování etických principů při přípravě vysokoškolských závěrečných prací.

In Prague on January 11, 2016 .....

Abstract

The amount of NH_3 stored on the walls of Selective Catalytic Reduction (SCR) systems is an interesting parameter for utilization in urea injection control. However, it has to be estimated as it cannot be measured onboard vehicle.

This thesis introduces the state of the art in modeling and estimation of SCR systems by reviewing the published literature. Further, it proposes a nonlinear physics-based SCR catalyst model and Extended Kalman Filter (EKF) for online estimation of outlet specie concentrations and NH_3 storage.

Simulations over standardized driving cycle show the designed model provides accurate open-loop predictions and the EKF further slightly improves them. A robustness analysis shows that, despite sensitivity to inputs, EKF introduces significant benefit over open-loop model simulations.

Abstrakt

Množství amoniaku (NH_3) usazeného na stěnách katalyzátorů pro Selektivní katalytickou redukci (SCR) je parametr zajímavý pro využití v řízení vstřikování močoviny. Tento parametr však nelze měřit během provozu, může být pouze odhadován.

Tato diplomová práce představuje současnou úroveň modelování a odhadování SCR systémů průzkumem literatury. Dále představuje nelineární model SCR katalyzátoru založený na fyzice a rozšířený Kalmanův Filtr (EKF) pro odhadování výstupních koncentrací látek a množství usazeného NH_3.

Simulace přes standardizovaný jízdní cyklus ukazují, že navržený model poskytuje přesné predikce a EKF je dále mírně vylepšuje. Analýza robustnosti ukazuje, že i přes citlivost na vstupní hodnoty, EKF přináší výraznou výhodu oproti simulacím modelu v otevřené smyčce.

Contents

List of acronyms

AMOX	Ammonia oxidation catalyst
ANR	Ammonia to NO_x ratio
CARB	California's Air Resource Board
CFD	Computational Fluid Dynamics
CH_4	Methane
CO_2	Carbon dioxide
CPU	Central processing unit
CSTR	Continuous stirred-tank reactor
DAE	Differential algebraic equation
DEF	Diesel exhaust fluid
CSTR	Diesel oxidation catalyst
DPF	Diesel particulate filter
ECU	Engine control unit
EGR	Exhaust gas recirculation
EKF	Extended Kalman Filter
EPA	(United States) Environmental Protection Agency
ETC	European transient cycle
EU	European Union
FTP	Federal test procedure
HC	Hydrocarbons
HCHO	Formaldehyde
HNCO	Isocyanic acid
LNT	Lean NO_x trap
MPC	Model Predictive Control

N_2O	Nitrous oxide
NH_3	Ammonia
NH_3^*	Ammonia adsorbed on catalyst walls
NMHC	Non-methane hydrocarbons
NMOG	Non-methane organic gas
NMPC	Nonlinear Model Predictive Control
N_2	Nitrogen
NO	Nitric oxide
NO_2	Nitrogen dioxide
NO_x	Nitrogen oxides, includes NO and NO_2
O_2	Oxygen
OBD	On-Board Diagnostics
PDE	Partial differential equation
PEMS	Portable Emission Measurement System
PI	Proportional-Intergral (controller)
PID	Proportional-Intergral-Derivative (controller)
PM	Particulate matter
PN	Particle number
RMS	Root mean square
SCR	Selective Catalytic Reduction
SCR/DPF	Combined SCR and DPF
SOF	Soluble liquid fraction
TWC	Three-way catalyst
US	United States
WHSC	World Harmonized Stationary Cycle
WHSC	World Harmonized Transient Cycle
WLTC	World-wide harmonized Light duty driving Test Cycle

List of symbols

a	algebraic variables
A_f	frontal flow area [m^2]
A_i	Arrhenius factor's pre-exponential coefficient of ith reaction
E_i	Arrhenius factor's activation energy of ith reaction [J mol^{-1}]
C_i	concentration of ith chemical specie [mol m^{-3}]
$C_{i_{\text{in}}}$	inlet concentration of ith chemical specie [mol m^{-3}]
C^{ppm}	chemical specie concentration [ppm]
D	diagonal factor of error covariance matrix
f	nonlinear continuous-time system function
f_k	nonlinear discrete-time system function
F_k	system function Jacobian evaluated at time k
h	nonlinear continuous-time output function
h_k	nonlinear discrete-time output function
H_k	output function Jacobian evaluated at time k
k_i	Arrhenius factor of ith reaction
$k\|k-1$	estimate at time k based on measurements from time $k-1$
$k\|k$	estimate at time k based on measurements from time k
K_{cs}	NO_x sensor's cross-sensitivity factor to NH_3 [-]
L	catalyst length [m]
M	NH_3 storage capacity [mol m^{-3}]
M_{gas}	Molar mass of exhaust gas [kg mol^{-1}]
$\dot{m}$	exhaust mass flow [kg s^{-1}]

N	number of axial elements [-]
P	error covariance matrix
P_{in}	inlet pressure [Pa]
Q_{cov}	process noise covariance matrix
r_i	reaction rate of ith reaction [mol m^{-3} s^{-1}]
R	ideal gas constant [J K^{-1} mol^{-1}]
R_{cov}	measurement noise covariance matrix
S	free space for NH_3 adsorption
S_r	reaction source term [mol m^{-3} s^{-1}]
σ	stoichiometric coefficient [-]
t	time [s]
Δt	sampling time [s]
T	temperature [K]
θ	NH_3 coverage ratio [-]
θ_i	NH_3 coverage ratio of ith NH_3 storage site [-]
θ_{tot}	total NH_3 coverage ratio of all sites [-]
u_k	system inputs at time k
U	unit upper triangular factor of P
v	flow velocity [m s^{-1}]
v_k	measurement noise at time k
w_k	process noise at time k
x_k	system states at time k
y_k	system outputs at time k

Chapter 1

Introduction

Increasingly stringent emissions standards are driving automobile manufacturers to optimize their engines and invest in exhaust-gas aftertreatment systems. Diesel Particulate Filter (DPF), as the most effective exhaust gas aftertreatment device for removing particulate matter, nowadays features in all diesel-engine vehicles sold in the developed markets. Three-way catalysts (TWC) and Diesel oxidation catalysts (DOC) have been used for decades to treat emissions of unburnt hydrocarbons (HC) and carbon monoxide (CO). TWC can additionally treat NO_x for rich-burn engines, but lean-burn engines—including the diesel engine—require alternative solutions in the form of Lean NO_x trap (LNT) or Selective Catalytic reduction (SCR).

The purpose of SCR catalysts is to reduce nitrogen oxides (NO_x) to nitrogen and water. They require a reducing agent in the form of ammonia (NH_3), which is provided through injection of liquid urea solution into exhaust gas at the upstream of the SCR. The surface-type NO_x reducing reaction require the gas-phase NH_3 to adsorb on the walls of the catalyst.

The amount of ammonia (NH_3) stored on the walls of SCR catalyst significantly affects NO_x conversion efficiency and outlet NH_3 slip. This makes NH_3 storage interesting for utilization in urea injection control. However, NH_3 storage is not directly measurable onboard vehicle, it can only be estimated. Model-based online estimation requires models that can run on in-vehicle hardware while being able to capture the main phenomena of SCR operation with sufficient accuracy.

This thesis introduces the state of the art in modeling and estimation of SCR systems by reviewing the published literature. Further, it proposes a nonlinear physics-based SCR catalyst model and Extended Kalman Filter (EKF) for online estimation of outlet specie concentrations and NH_3 storage. Simulations over WLTC driving cycle show that the designed model provides accurate open-loop predictions. The EKF further reduces maximum and root mean square error. A robustness analysis shows that, despite sensitivity to inputs, EKF introduces significant benefit over open-loop model simulations.

I organized the contents of the thesis as follows: Chapter 2 serves as an introduction to the existing vehicle emission treatment solutions, and the emission regulations that drive their development. Chapter 3 discusses the SCR catalyst in more detail and introduces the combined SCR and DPF catalyst. Chapter 4 summarizes the relevant literature on modeling and estimation of SCR and SCR/DPF catalysts to introduce the state of the art. Chapter 5 presents a design of two lower-fidelity models of SCR catalyst and validates their predictions against calibrated high-fidelity SCR model. Chapter 6 describes design of Extended Kalman filter and discusses the estimation results and estimator's robustness to perturbations of inputs and internal states. Finally, Chapter 7 provides some concluding remarks.

Chapter 2

Diesel Engine Emission Control

Emission of pollutants from vehicles into the environment can be prevented either by engine improvements and modifications to minimize production of emissions during combustion by introducing advanced injection and control approaches, or by utilizing aftertreatment systems to remove pollutants from the exhaust gas. This chapter briefly discusses the means of emission control as outlined above and introduces emission standards, which are the main driving force of the change to cleaner transportation.

2.1 Emissions and regulations

Vehicular emissions comprise a significant portion of the total global emission output. They include not only greenhouse gases potentially contributing to global warming, but several other gaseous pollutants found to have adverse health effects on human body as well.

Primarily, emissions of CO, NO, NO_2, unburnt hydrocarbons (HC) and particulate matter (PM) are subject to regulation. Ammonia, a secondary emission of aftertreatment systems, is regulated in European EURO VI heavy duty standard [1]. Since aftertreatment systems are sensitive to sulfur content in the fuel, it is subject to regulation as well.

Carbon dioxide emissions limits have been introduced in Europe for passenger cars in 2009 [2]. This put more pressure on the engine manufacturers to increase efficiency of the engines as CO_2 production is directly proportional to fuel consumption. With even more stringent requirements already planned for the future, this may lead to faster introduction of other than internal combustion engines or hybrid combinations.

Tightening up on the vehicular emissions limits is driven by the US and European Union, other countries generally adapt modifications of US or EU standards with a few years delay. United states emissions standards are maintained on the federal level by Environmental Protection Agency (EPA), but several states implement more stringent rules maintained by California's Air Resource Board (CARB). Emission standards are issued separately for light-duty vehicles (passenger cars, light commercial vehicles), heavy-duty vehicles (trucks, buses) and non-road vehicles (agricultural, mining vehicles). European union issues different limits for gasoline and diesel engine vehicles. Neither in US or EU is implementation of specific emission control approach mandated by the laws and it is left subject to manufacturer's decision.

Vehicular emissions are measured under laboratory conditions by standardized driving cycle tests. There are different tests for heavy-duty and light-duty vehicles and various driving conditions. While international driving cycle tests are under development, emissions are tested for

certification differently around the world. Recently, several studies reported a big difference between the driving cycle test emissions and real-world driving emissions [3]. This triggered attention of the European commission and PEMS (Portable Emission Measurement System) testing is planned to be included in the vehicle emissions certification process [4].

2.1.1 Heavy-duty vehicles

Table 2.2 summarizes heavy-duty vehicle emission standards introduced in the last two decades in Europe and Table 2.1 for selected years in the US. The biggest improvement has been achieved for emissions of NO_x and PM in both US and Europe. Emission limits are not directly comparable, because they are set for different driving cycles, but US emissions are generally more stringent than European. EURO VI introduced in 2014 are said to be comparable with US 2010 standards [5], which were phased-in between 2007–2010 [6]. EURO VI additionally incorporate ammonia slip and particle number limits. CO_2 emissions are not regulated in heavy-duty vehicles.

Level	CO	HC	NO_x	PM	
				general	buses
US 1991	15.5	1.3	6	0.25	
US 1994	15.5	1.3	5	0.1	0.07
US 1998	15.5	1.3	4	0.1	0.05
US 2004	15.5	2.4		0.1	0.05
US 2010*	15.5	0.14	0.2	0.1	0.05

Table 2.1: US EPA Heavy duty diesel emission standards. All values are in g/bhp.h. Table shows maximum allowed emissions during a standardized FTP driving cycle. US 2010 standards were phased-in between 2007–2010. There are additional Not to Exceed requirements in US 2010 standards [6].

Tier	Year	Op. conditions	CO	HC	NMHC	CH_4	NO_x	PM	PN	Smoke
EURO I	1992	Steady state	4.5	1.1	-	-	8	0.36		
EURO II	1998	Steady state	4	1.1	-	-	7	0.15		
EURO III	2000	Steady state	2.1	0.66	-	-	5	0.1		
		Transient	5.45	-	0.78	1.6	5	0.16		
EURO IV	2005	Steady state	1.5	0.46	-	-	3.5	0.02		0.8
		Transient	4	-	0.55	1.1	3.5	0.03		
EURO V	2008	Steady state	1.5	0.46	-	-	2	0.02		0.5
		Transient	4	-	0.55	1.1	2	0.03		
EURO VI	2014	Steady state	1.5	0.13	-	-	0.4	0.01	8×10^{11}	
		Transient	4	-	0.16	0.5	0.46	0.01	6×10^{11}	

Table 2.2: EU Heavy duty diesel emission standards. Particle number (PN) is in 1/kWh, smoke in 1/m, other emissions in g/kWh. Table shows maximum allowed emissions during a standardized driving cycle. NMHC denotes non-methane hydrocarbons. For steady state EURO I and EURO II limits are defined over ECE R-49, for EURO III to EURO V over ESC & ELR and EURO VI over WHSC, for transient standards EURO III to EURO V ETC cycle is used and for EURO VI WHTC [5, 7].

2.1.2 Light-duty vehicles

US EPA's first Tier 1 emission standards were issued in 1991 and fully phased-in in 1997. Tier 2 standards were introduced in 2004 and were fully phased-in by 2009. As of 2015, Tier 2

standards are in force. There are 11 bins, Bin 11 to Bin 1 with increasingly stringent limits. All vehicles must comply with at least Bin 11 standard, the whole fleet (based on sales) must comply with Bin 5 on average. Since 2008 bins 9-11 are phased-out. Table 2.4 summarizes the standards. Tier 3 standards are expected to be phased-in between 2017–2025, after fully phased-in vehicle emissions will be reduced by 60% - 80% compared to Tier 2 [8].

European union issued their first Euro 1 standard in 1992. The latest Euro 6 came into force in 2014 for new models and from September 2015 for all cars sold. See Table 2.3 for summary. As of January 2015, any subsequent standards have not been proposed yet, but can be expected around 2020 [4].

Carbon dioxide restrictions have been introduced in the EU in 2009 for passenger cars with a goal to reach 130 g/km by 2015 (which has been met in 2013) and 95 g/km by 2021. US laws target 139 g/km and 88 g/km by 2016 and 2025, respectively [9].

Light-duty vehicles besides passenger cars include larger vehicles as well, such as trucks and vans, EU specifies separate limits for light commercial vehicles and US EPA Tier 2 and upcoming Tier 3 standards are structured into several categories based on vehicle weight. For complete summary of light-duty standards see [8].

Tier	Year	Engine	CO	HC	HC+NO_x	NO_x	PM	PN
Euro 1	1992	Diesel	2.72		0.97		0.14	
		Gasoline	2.72		0.97			
Euro 2	1996	Diesel	1.0		0.7		0.08	
		Gasoline	2.2		0.5			
Euro 3	2000	Diesel	0.64		0.56	0.5	0.05	
		Gasoline	2.3	0.2		0.15		
Euro 4	2005	Diesel	0.5		0.3	0.25	0.025	
		Gasoline	1.0	0.1		0.08		
Euro 5	2009	Diesel	0.5		0.23	0.18	0.005	
		Gasoline	1.0	0.1		0.06	0.005	
Euro 6	2014	Diesel	0.5		0.17	0.08	0.005	6.0×10^{11}
		Gasoline	1.0	0.1		0.06	0.005	6.0×10^{11}

Table 2.3: European passenger car emission standards. Particle number (PN) value is particles per kilometer, all other values are in g/km. PN limit for gasoline engines is for direct injection engines only [10].

Cat.	Year	Life	Total HC	HCHO	NMHC/ NMOG	CO	NO_x diesel	NO_x gasoline	PM
Tier 1	1991	intermediate	0.41		0.25	3.4	1.0	0.4	0.08
		full useful			0.31	4.2	1.25	0.6	0.1
Tier 2 Bin 8	2004	intermediate		0.15	0.1	3.4		0.14	0.02
		full useful		0.18	0.125	4.2		0.2	0.02
Tier 2 Bin 5	2004	intermediate		0.15	0.075	3.4		0.05	0.01
		full useful		0.18	0.09	4.2		0.07	0.01

Table 2.4: US passenger car standards. All in g/mile. Intermediate life stands for first 50 000 miles or 5 years, whichever comes first, full useful life is 100 000 miles or 10 years. HCHO denotes formaldehyde and NMHC non-methane HC (for diesel engines), NMOG stands for non-methan organic gas (for gasoline engines) [8].

2.2 In-engine emission treatment

Emission production can be minimized by improved fuel-air mixing and injection timing. Engines with carburetors were replaced during 1980's by single point injection engines. These were replaced by engines utilizing multi-port injection approach and direct injection. Improvements in engine design, materials and control play a significant role in emission reduction.

Exhaust gas recirculation (EGR) is used to route controlled portion of the exhaust gas back to the engine inlet. It is customary to cool it down first to increase its density to allow more exhaust gas to be returned. Since the chemical composition of the exhaust gas, which comprises mainly CO_2 and water vapor, has higher specific heat than air, lower combustion temperatures are achieved and therefore less NO_x is produced. Exhaust gas also dilutes the nitrogen content of the air, which also leads to the decrease of NO_x production. EGR comes in two varieties: a high-pressure EGR—which takes the exhaust gas downstream of the engine—and a low-pressure EGR, which routes back exhaust gas from downstream of the turbocharger or even aftertreatment systems [11]. The downside of the exhaust gas recirculation is a slight decrease in the power of the diesel engine and increased fuel consumption and particulate matter production, which has to be compensated by simultaneous use with particulate filter [12].

Exhaust gas recirculation (EGR) has been introduced more than 40 years ago, but it took until 1990's to early 2000's to become a widely used technique to lower NO_x diesel emission [13]. The deployment of EGR was motivated by implementation of increasingly stringent NO_x emission standards in the US and Europe. Under emission standards introduced in late 2000's, using EGR alone is not sufficient to meet the NO_x removal requirements, thus making its combined deployment with SCR systems a common solution [13]. Some very recent configurations exclude EGR and rely on SCR only [14].

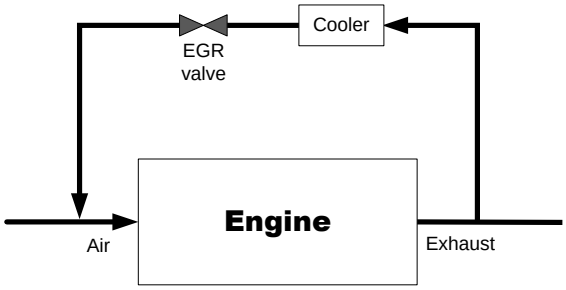

Figure 2.1: Exhaust gas recirculation. Portion of the exhaust gas is cooled and routed back to engine inlet to lower combustion temperature and NO_x production.

2.3 Particulate matter filtration

Diesel particulate filter (DPF) is the most effective exhaust gas aftertreatment device for particulate matter (PM) removal. The particulate matter is a product of incomplete combustion. It comprises solid soot particles, which are captured in the microscopic pores of the filter walls. The filter has to be periodically or continuously regenerated, i.e. the soot particles have to be burnt-off to prevent clogging and to allow continued operation.

Diesel particulate filters have been introduced to the market in late 1980's for non-road vehicles and retrofit of heavy-duty vehicles. With the introduction of increasingly stringent vehicle emission standards over the years, they have become an integral part of the diesel emission exhaust after-treatment systems not only for heavy-duty vehicles, but for light-duty vehicles as well. The first manufacturer to implement DPF filter into passenger car was PSA Peugeot

Citroën in 2000 [15], which met the EURO 4 norm four years before it came into force. DPF filters offer excellent particle filtration with efficiency around 90% with respect to particle mass [4]. The deployment of exhaust gas recirculation (EGR) to treat NO_x emissions further raised importance of DPF as EGR significantly increases soot production.

2.3.1 Particulate matter

Particulate matter is produced during incomplete fuel combustion. It comprises soot particles (in solid phase), soluble liquid fraction (SOF) and sulfate fraction (both in condensed phase) [15]. Most of the mass of the particulate matter is down to the soot particles. The soot particle size is in the range of 100 – 500 nm and this is where DPF achieves filtration efficiency well over 90% with respect to mass. Condensed phase particles, even though they amount to very little mass, constitute more than 90% of the total particulate matter with respect to number of particles. They are of very small size in the range of 5 – 20 nm. DPF's have limited capability in filtering such small particles [16]. Oxidation catalyst upstream of the DPF improves filtration of the SOF for the cost of increased sulfate slip. This can be minimized by using very low-sulfur diesel fuel.

2.3.2 Filtration

Pore dimensions of the filter are much larger than size of the particulate matter. *Sieve*-type filtration where larger particles get stuck in a smaller pore is therefore not viable, but instead *cake* and *deep-bed* filtration types are utilized. Agglomerates of smaller-sized particles are caught in filter's pores to create a so called soot cake. With growing cake size the efficiency of cake filtration is improved for the cost of increased pressure drop. The particles can also get attached to filter walls by diffusion and impaction, which is collectively termed as deep-bed filtration. This type of filtration is less effective than the cake-filtration, but it does not significantly add-up to the filter's back-pressure.

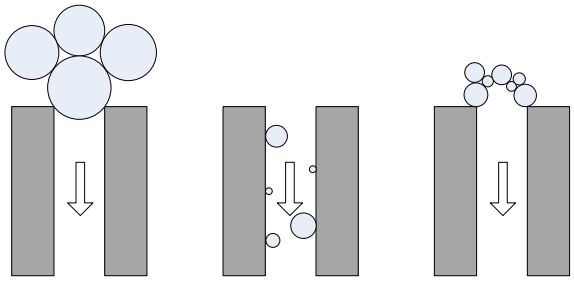

Figure 2.2: Filtration modes. In *sieve* mode (left), larger particles are captured in smaller pores, in *deep-bed* mode (middle) particles get attached to the filter walls, and in *cake* mode (right) agglomerates of smaller-sized particles are caught in filter's pores and create a soot cake. Arrows denote airflow direction [16].

2.3.3 Structures and materials

Diesel particulate filters come in many varieties. There are fiber filters that utilize either ceramic or metallic fibers, ceramic foam filters, paper filters, fabric filters and other. The most common are ceramic wall-flow filters. Wall-flow filter is a modification of a flow-through filter used for catalytic converters. It comprises a multichannel honeycomb-shaped monolith with every channel open from one side and plugged from the other. The channels are oriented and distributed in a chessboard-pattern as is depicted in Fig. 2.3. This design forces the exhaust

gas to flow through the filter walls. Typical size of the wall-flow monolith is 144 mm in diameter and 152 mm in length [16]. The wall-flow monoliths are commonly produced from cordierite or silicon carbide. Cordierite is a well known material, which has been for decades used in production of catalytic converters. It is a relatively cheap material with low thermal expansion. However, cordierite has a low melting point of about 1200 °C, which makes silicon carbide the preferred material choice of many manufacturers, because high temperatures are needed during regeneration of the filter. Silicon carbide's melting point is about 2700°C, but it suffers more from thermal expansion than cordierite.

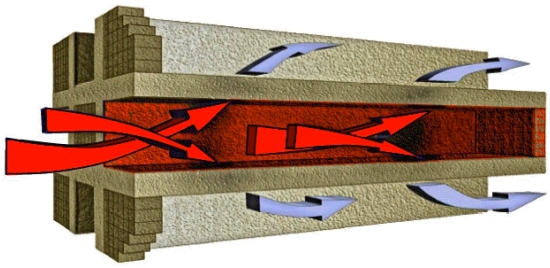

Figure 2.3: Wall-flow monolith. Honeycomb-shaped wall-flow filter used for DPF [17] .

2.3.4 Regeneration

Regeneration is a removal process of the soot accumulated in the filter. It is required by the filter to prevent clogging and to allow sustained operation. Regeneration is carried out thermally by burning off the accumulated soot (mostly carbon) by oxidation with NO_2 molecules. Limited soot burn-off, which naturally occurs in the filter, can be boosted by oxidation of NO to NO_2 as well as by lowering the required burn-off temperature. This can be achieved passively by using catalysts, which can either be directly applied on the filter walls in a form of catalytic washcoat or added to the fuel. Platinum is commonly used as the washcoat catalyst, cerium can be used as the fuel-borne catalyst [15]. Active approach aims at increasing the temperature in the filter to promote the burn-off. This can be achieved by late-fuel injection during the combustion, which increases exhaust gas temperature, or by injecting the fuel-air mixture directly into the exhaust gas. Commercial applications often combine both active and passive approaches to trigger the regeneration. For long-distance highway driving DPF can be designed to regenerate passively, for city-driving, where high enough exhaust gas temperatures are not achieved for sufficiently long period to allow regeneration, active approach is required.

2.4 Carbon monoxide and hydrocarbons treatment

Catalytic converters are the oldest exhaust gas treatment technology. Two-way catalytic converters oxidate carbon monoxide and unburnt hydrocarbons to carbon dioxide and water. Three-way catalytic converters in addition to the oxidation reactions are also able to reduce NO_x to oxygen and nitrogen. Since the reduction is possible only at rich operating conditions, three-way catalysts are utilized mainly with gasoline engines while diesel engine NO_x emissions have to be treated differently. The two-way catalytic converters used for diesel engines are called diesel oxidation catalysts (DOC). The catalytic converters comprise inert carrier, a honeycomb-shaped flow-through monolith, usually made out of cordierite, and a catalytic washcoat. Noble metals, such as platinum, rhodium and palladium are used as the active catalysts.

2.5 Nitrogen oxides removal

Three-way catalytic converters have been used for treating nitrogen oxide NO_x emissions for rich-burn engines since 1980's. For lean-burn engines, such as diesel engines, exhaust gas recirculation (EGR) and subsequently selective catalytic reduction (SCR) catalysts and lean NO_x traps have been introduced.

Lean NO_x trap (LNT), also called NO_x adsorber is a competing technology to the SCR. In contrast to the SCR it does not require injection of a reducing agent into the system to allow NO_x conversion. LNT operates in two periods, rich and lean. During the lean period the noble-metal impregnated washcoat oxidizes NO to NO_2 and a storage material catalyzed with an alkaline earth metal (e.g. barium) adsorbs the NO_x molecules. During the rich period LNT is regenerated, stored NO_x desorbs and is reduced on the washcoat to N_2. Lean NO_x traps have to be periodically desulfated by rising the temperatures to about 700 °C. LNT's are the primary choice for NO_x treatment in light duty vehicles with smaller engines, where they are cheaper than the SCR [18]. For larger engines and heavy duty vehicles SCR is the preferred choice.

Ammonia produced by the LNT can be utilized by a downstream SCR, thus making it possible to create a urea-free deNO_x system. There are commercial applications utilizing LNT+SCR configuration [19], but it mostly remains a technology for the future [20]. For more discussion on SCR and combined SCR/DPF filter see the following chapter.

2.6 Secondary emissions control

Ammonia, a toxic substance used as NO_x reducing agent, can slip away from the SCR catalyst if its dosing is not matched properly to the driving conditions. EURO VI norm for heavy-duty applications sets a 10 ppm limit over WHSC and WHTC cycles [1]. Nitrous oxide (N_2O) is a product of various aftertreatment systems including DOC, SCR and ammonia slip catalyst. It has been recognized as a strong greenhouse gas and is subject to regulation under greenhouse gas rule in th US [20]. While ammonia can be oxidized by an ammonia oxidation catalyst, production of N_2O is minimized by better aftertreatment system design and temperature control.

Ammonia oxidation catalyst (also called ammonia slip catalyst or clean-up) comprises a zeolite-based NH_3 storage layer and a platinum-group-metal oxidation layer over which several reactions compete for the ammonia molecules [21]. About 75% of ammonia can be converted to harmless N_2, but the remainder results in NO_x and a small amount of N_2O [20].

Chapter 3

Selective Catalytic Reduction Systems

This chapter introduces two applications of selective catalytic reduction (SCR) in automotive aftertreatment systems for NO_x reduction: SCR catalyst and combined SCR/DPF catalyst. The discussion covers operating principles, urea injection, chemical reactions, materials, controls, and finally, interaction between SCR and DPF functionalities in the combined device. Succeeding Chapter 4 discusses modeling and estimation, and completes the introduction to the SCR systems.

3.1 SCR catalyst

For engines operating in lean-burn mode, the non-selective approach for treating NO_x is not viable due to high oxygen content in the exhaust gas. Therefore, three-way catalysts are not used for lean-burn gasoline engines and diesel engines. Researchers turned their attention to selective catalytic reduction approach, where NO_x reduction on the catalyst-covered walls of the converter is selectively promoted by injecting a reducing agent. Unsurprisingly, hydrocarbon based approach has been studied intensively as hydrocarbon can be simply added by fuel-injection into the exhaust gas [22]. Hydrocarbon based approach has shown only poor NO_x conversion and attention was switched to the most selective catalytic reduction approach known to reduce NO_x—ammonia-based selective catalytic reduction—a well-known approach used in stationary processes including chemical plants and power plants.

Selective catalytic reduction (SCR) for the treatment of NO_x in the vehicle exhaust gas uses urea to selectively promote chemical reactions that convert NO_x to harmless nitrogen molecules and water. Urea is injected into the exhaust gas where it is converted to ammonia, which acts as the reducing agent for NO_x conversion on the catalyst walls, which are impregnated with catalytic materials to boost the reduction.

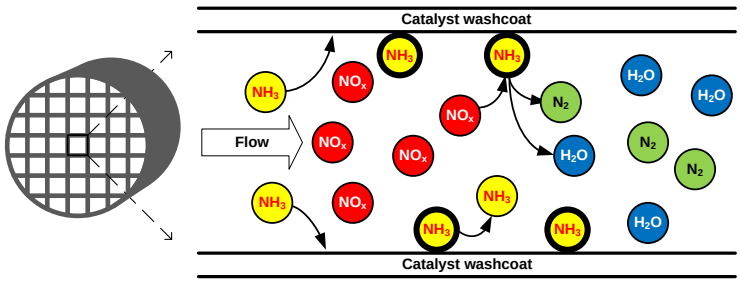

Figure 3.1: Single channel of a flow-through SCR catalyst. Ammonia (NH_3) adsorbs on the catalyst walls, where it participates in reduction of gas-phase NO_x into nitrogen and water; adsorbed species are denoted in bold.

Adoption of urea necessitates inclusion of additional components into the vehicle to handle its storage, dosing and injection; this increases production costs. However, SCR's high NO_x conversion allows for reducing or even complete omission of EGR in certain engine & aftertreatment configurations [14], thus improving fuel efficiency of the vehicle.

3.1.1 Chemical reactions

Three surface-type reactions are responsible for most of the NO_x reduction in SCR catalyst. These reactions require ammonia adsorbed on the catalyst walls. The two-way conversion between gas-phase and adsorbed NH_3 is described by the following NH_3 adsorption/desorption mechanism

$$NH_3 + S \longleftrightarrow NH_3^* \tag{3.1}$$

where S denotes a free site on the catalyst wall to which gas-phase NH_3 is adsorbed. The reactions below are referred to as standard (3.2), fast (3.3) and slow (3.4), with respect to their relative reaction rates [23]:

$$4\,NH_3^* + 4\,NO + O_2 \longrightarrow 4\,N_2 + 6\,H_2O \tag{3.2}$$
$$2\,NH_3^* + NO + NO_2 \longrightarrow 2\,N_2 + 3\,H_2O \tag{3.3}$$
$$8\,NH_3^* + 6\,NO_2 \longrightarrow 7\,N_2 + 12\,H_2O \tag{3.4}$$

Standard reaction in eq. (3.2) dominates when the catalyst operates at standard diesel engine-out exhaust gas NO_2/NO_x ratio, when 70-90% emissions of nitrogen oxides are in the form of NO [24]. Fast reaction (3.3) becomes dominant when NO_2/NO_x ratio is around 0.5, e.g. in aftertreatment configurations with oxidation catalyst upstream of SCR. At this NO_2/NO_x ratio the SCR catalyst is the most efficient. If the concentration of NO_2 exceeds that of NO then the extra NO_2 has to be reduced through the slow reaction (3.4) and the total NO_x conversion efficiency declines.

Furthermore, oxidation of NO to NO_2 and a number of undesired reactions are taking place in the SCR, e.g. oxidation of adsorbed NH_3 to N_2 or NO, formation of NH_4NO_3 (ammonium nitrate) and N_2O (nitrous oxide) [23].

3.1.2 Catalyst and materials

SCR catalysts for automotive applications are manufactured as honeycomb-shaped flow-through monoliths as depicted in Fig. 3.2. Monoliths are either produced from a catalytic

material as a whole or catalytic substances are applied as a washcoat on a monolith made from non-catalytic substrate. The second method is preferred, because lower quantities of catalytic substances are needed to achieve comparable NO_x conversion, thus making the catalyst cheaper.

The most common materials used to make the inert substrate are aluminum titanate Al_2O_3 or titanium oxide TiO_2 and their modifications. These materials can be also used to prepare the washcoat by mixing them with the active catalytic substances such as vanadium pentoxide V_2O_5 or tungsten trioxide WO_3. Another approach is to washcoat the inert substrate with zeolites, sponge-like minerals with extensive microporous structure. They are exchanged with base metals, most commonly copper or iron, that serve as the catalysts. Zeolite-based catalysts have better thermal durability, which allows them to be used at high temperatures such as those reached during DPF regeneration, thus making it possible to deploy SCR catalyst downstream of the DPF. With high-sulfur diesel—available on markets in developing countries—vanadium-based catalysts outperform sulfur-sensitive zeolite-based devices [25].

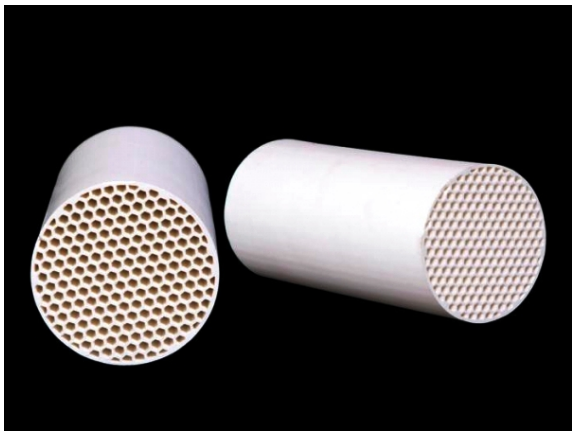

Figure 3.2: SCR monolith. Honeycomb-shaped flow-through monolith for SCR catalysts [26] .

Apart from the already mentioned high-temperature durability and sulfur sensitivity, there are many other factors to be considered for material selection, such as low-temperature performance, thermal expansion, NO_x conversion at different temperatures, ageing rate, ammonia slip and production of secondary emissions.

3.1.3 Urea injection

Ammonia (NH_3) used in stationary SCR applications is not suitable for in-vehicle use, where its safe handling might be impossible to guarantee. Instead of toxic ammonia a 32.5%-by-weight solution of solid urea and deionized water, marketed under the names of *DEP* in the US and *AdBlue* in Europe, has been chosen as the reducing agent for the SCR catalysts.

Urea is a non-toxic, environment-friendly substance, which has been industrially produced for many decades for agricultural purposes. Therefore only distribution of the urea solution to the SCR-using vehicles introduces a new problem. It can either be supplied in bulk to the fueling stations or distributed to the customer in polyethylene bottles with volume ranging from 5 to 18 liters. The freezing temperature of the solution is -11°C and the phase change does not spoil it [18].

According to [18] the consumption of urea in heavy duty applications is around 1% compared to the fuel consumption. For a vehicle with a tank size of around 75 liters, one fill should last about 25 000 km. For light duty applications the urea consumption is around 2%, with a tank size of up to 28 liters the travel distance reaches around 17 000 km without a need to refill.

The aqueous urea is injected into the hot exhaust gas where water evaporates (3.5a) and solid urea is via subsequent decomposition (3.5b) and hydrolyzation (3.5c) converted to ammonia and CO_2. During the process, isocyanic acid (HNCO) is created and consumed.

$$NH_2{-}CO{-}NH_2(\text{liquid}) \longrightarrow NH_2{-}CO{-}NH_2(\text{solid}) + H_2O \tag{3.5a}$$

$$NH_2{-}CO{-}NH_2(\text{solid}) \longrightarrow NH_3 + HNCO \tag{3.5b}$$

$$HNCO + H_2O \longrightarrow NH_3 + CO_2 \tag{3.5c}$$

Urea is supplied from the tanks by a dosing pump or separately by a pump and a dosing device. The dosing can be also performed in the injector. The best SCR performance is observed when proper amount of urea is injected atomized into small particles and thoroughly mixed with the exhaust gas.

Spraying the urea in small particles allows for better conversion to ammonia with minimal production of isocyanic acid and other chemicals as byproducts that are either harmful to the environment or that pose a risk for the urea injection and dosing system itself by creating solid deposits, for instance in the injector nozzle. There are two major approaches of urea injection: air assisted and airless. The air assisted approach allows for better atomization of the urea, but for the cost of having extra components associated to air compression. The airless approach is less complex, but requires higher injection pressure to achieve required atomization and is more prone to creation of solid deposits. To prevent crystallization of urea due to water evaporation caused by high temperatures, the injector nozzle is cooled [27].

Proper mixing makes the distribution of the reactants on the SCR more uniform, thus allowing every channel of the catalyst to have appropriate amount of reactants. Non-uniform distribution of ammonia leads to sub-optimal NO_x reduction in channels with insufficient ammonia, and to ammonia-slip in channels with excess of ammonia. Proper mixing can be achieved by having sufficiently long exhaust pipe between the urea injection point and the SCR catalyst, but most of the applications incorporate mixers, either upstream or downstream of the injection point, to increase turbulence of the exhaust gas.

Due to relatively high freezing temperature of aqueous urea at about -11°C, it is necessary to allow for unfreezing the solution when used in colder climate. Injection and dosing systems are designed to prevent urea from freezing in the pipes, usually by flushing the system after operation.

3.1.4 Sensitivity to inputs

As discussed above, NO_2/NO_x ratio determines rates of NO_x reducing reactions (3.2)— (3.4), and subsequently affects overall NO_x conversion efficiency. Further, NH_3/NO_x ratio—often abbreviated as ANR (ammonia to NO_x ratio)—determines whether there is enough NH_3 for NO_x conversion. Standard and fast reactions consume equal amounts of NH_3 and NO_x. Since slow reaction requires ANR = 1.25 and undesired reactions—such as NH_3 oxidation or formation of solids—consume NH_3, the optimal ANR is slightly above 1, but does not remain fixed during operation as it further depends on operating conditions. Another parameter that

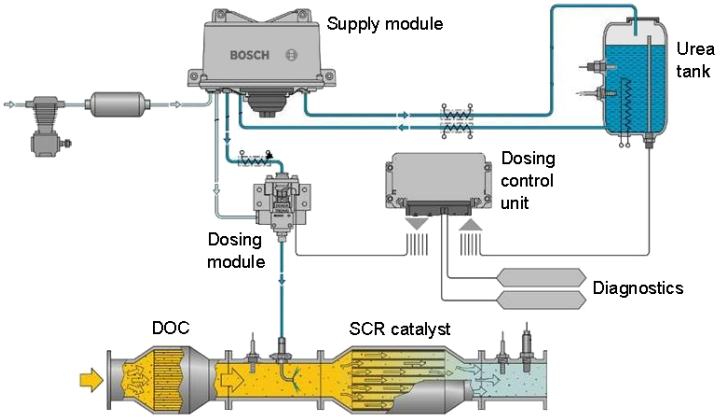

Figure 3.3: Urea injection system. Urea dosing and injection in SCR system by Bosch [28].

affects NO_x conversion efficiency is exhaust gas flow rate, which determines the time available for chemical species to participate in the reactions before they leave the catalyst. The most influential input is temperature:

- chemical reaction rates depend exponentially on temperature
- NO_x conversion is not possible below light-off temperature
- urea may not completely decompose to NH_3 at low temperatures, and solid deposits are formed on the injector and inside the catalyst [27].
- undesired reactions—such as N_2O formation and oxidation of adsorbed NH_3—are stronger at high temperatures
- other influencing factors—e.g. NH_3/NO_x and NO_2/NO_x ratios—are temperature dependent [29], [30].

3.1.5 Control

Internal processes within SCR catalyst operate at very different timescales. While NH_3 adsorption and desorption reactions operate at fast sub-second time scale, NH_3 storage varies at the order of minutes, and catalyst performance is deteriorated by aging over years [31]. Moreover, SCR catalyst is a highly nonlinear system especially due to exponential temperature dependence of reaction rates. All of these factors make SCR difficult to control optimally over the whole operating range.

The traditional approach to SCR control, which aims at maximizing NO_x reduction efficiency, is open-loop control. It is able to achieve 60%-80% NO_x conversion efficiency [32] and meet up to EURO 5 emission standard [33]. However, open-loop control performs poorly in transients. Improvement can be achieved by introducing output feedback control utilizing PI or PID controllers with outlet NO_x sensor [32] and/or NH_3 sensor [34], however high price of NH_3 sensors discourages manufacturer's from their commercial application [35].

With more stringent emission standards the goal for the control of urea injection changed to maximizing NO_x conversion efficiency while bounding NH_3 slip at the SCR outlet. To guarantee bounded NH_3 slip, many extended their PI/PID output feedback control by model based NH_3 slip detection as in [34].

More accurate control for minimizing both NO_x and NH_3 at the SCR outlet can be achieved by state feedback control approach, which requires estimation of internal states, especially

NH_3 storage (NH_3 coverage ratio). This is a parameter with significant impact on both NO_x reduction efficiency and undesired ammonia slip of SCR catalysts. Another control approaches applied at SCR systems include adaptive control [36], model predictive control (MPC) [37] and more recently nonlinear model predictive control (NMPC) [38]. For more in-depth overview of SCR control see [31].

3.2 SCR/DPF catalyst

Most of the heavy-duty vehicles that comply with the EURO VI and US 2010 standards rely on combination of SCR and DPF to remove NO_x and particulate matter from the exhaust gas. Integration of SCR functionality on DPF filter promises possible advantages for the aftertreatment system [8]:

- Allows mounting both NOx reduction and PM filtering technologies closer to the engine, thus minimizing the heat loss, allows for faster SCR light-off, while making passive soot regeneration possible
- Removal of SCR and substituting DPF with SCR/DPF significantly lowers aftertreatment system volume, weight and cost with the downside of slightly lower total NOx conversion efficiency.
- Substituting DPF with SCR/DPF improves overall NOx conversion efficiency, while the number of catalysts and the volume of the aftertreatment system remain the same [39].

3.2.1 Catalyst

The combined SCR and DPF, often abbreviated as SCR/DPF or SCR-DPF, extends the wall-flow DPF filter with catalytic washcoat that promotes NO_x reduction. Catalysts that promote SCR reactions are washcoated mostly in the walls between channels or in the outlet channels [40]. NO_x reduction mechanism is similar to that of the flow-through SCR catalyst. SCR/DPF needs about three times the amount of catalytic washcoat to match the NO_x conversion of a comparable SCR catalyst. Since the exhaust gas has to pass through the catalyst walls, more porous monolith substrates have to be used to keep backpressure similar to that of DPF [20]. Fig. 3.4 shows the SCR/DPF wall-flow catalyst operation.

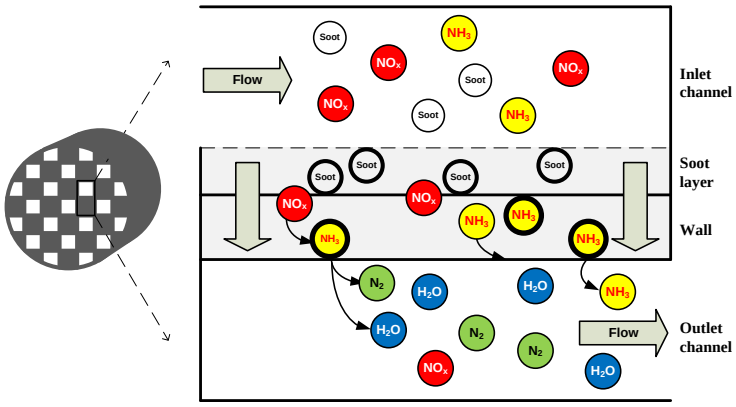

Figure 3.4: Wall-flow SCR/DPF catalyst. The porous wall is washcoated with catalytic material to promote NH_3 adsorption and NO_x conversion. Soot is captured in the pores of the wall and forms a soot cake in the inlet channel [20].

SCR/DPF monoliths are produced—similarly to DPF–from aluminium titanate, silicon carbide or cordierite. Material choice is be subject to the intended application: light duty or heavy

duty vehicles, active or passive PM regeneration, low-temperature operation or durability at higher temperatures, sensitivity to poisoning by sulfur or other contaminants and other.

3.2.2 SCR vs. DPF

Passive particulate matter (PM) oxidation and NO_x reduction are competing reactions in SCR/DPF, since both consume NO_2 from the exhaust gas. Passive PM regeneration is significantly inhibited by NO_x reducing reactions [41], this effect can be minimized by applying catalytic washcoat that facilitates NO_x reduction mostly to the filter walls and outlet channel rather than to the inlet channel. Another way is to design the filter to perform each task at different temperature range, i.e. require higher temperatures to perform the PM regeneration and lower temperatures to utilize the SCR functionality.

The influence of filtered PM on NO_x reduction is observed to be minimal in [42], [39]. Authors in [43], [44] suggested that NO_x conversion efficiency improves under PM loading conditions for NO_2/NO_x ratio > 0.5 and deteriorates for < 0.5. This is because SCR performs with the highest NO_x conversion efficiency at NO_2/NO_x around 0.5 and the improvement of the efficiency by passive PM oxidation is observed when it lowers the NO_2/NO_x ratio to the optimal value of 0.5. It is worth noting that authors in [43] have found that PM loading increases NH_3 storage compared to clean SCR/DPF, but opposite results were reported in [45]. This implies that more research is required to explain the influence of PM loading on NH_3 storage in SCR/DPF catalysts [41].

Chapter 4

Modeling and estimation of SCR: State of the art

This chapter introduces modeling of SCR catalysts and presents the state of the art with focus on computationally inexpensive control-oriented models that can be used for online estimation. The second section of this chapter provides an overview of model-based online estimation design approaches for SCR catalysts. Note that parts of the discussion in this chapter also appear in a proposed conference paper [46].

4.1 Modeling

Physics-based modeling approaches of SCR catalysts—complex devices involving many chemical and physical processes—are prevalent in the published literature. High-fidelity 3D models based on computational fluid dynamics (CFD) provide the most accurate description of SCR operation. Such models are used to study physicochemical phenomena in the catalyst, such as axial NH_3 distribution effects on SCR performance [47], sensitivity to inputs [48], or internal gas transport [49]. Simulation of high-fidelity models for the purposes of control design and calibration is computationally too expensive. Simpler models that consider only axial dimension of the catalyst or even zero-dimensional models are used for fast simulations on low-performance hardware, like vehicle ECU's. The following discussion concerns such models.

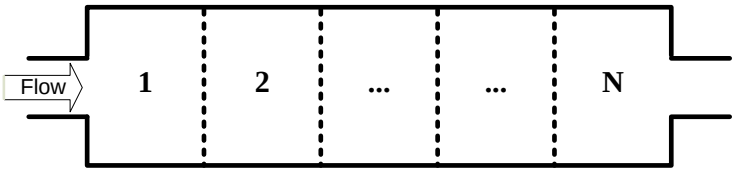

Figure 4.1: Channel discretization. Single-channel approximation of SCR catalyst discretized to N elements in the axial domain [50].

Fluid motion in a channel Single-dimensional models often consider the SCR catalyst as a single-channel, where a set of partial differential equations describes the fluid motion. The channel is spatially discretized to multiple axial elements—as Fig. 4.1 shows—to allow numerical simulation. Zero-dimensional models consider only single axial element, this is often equivalently formulated as continuous stirred-tank reactor (CSTR) model as in Fig. 4.2 [51]. Authors in [34] compared effects of spatial discretization on accuracy of their control-oriented

model to conclude that model accuracy is significantly affected by the number of axial elements. Reviewed publications generally consider 2 to 30 axial elements, Tab. 4.1 at the end of this section summarizes selected modeling studies. Besides the number of axial elements, selected discretization scheme affects accuracy of the discretized model. Chapter 5 includes comparison of several temporal and spatial discretization schemes.

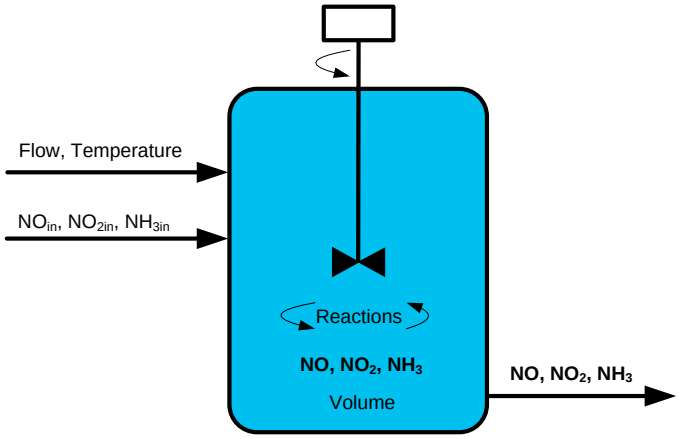

Figure 4.2: CSTR. A zero-dimensional continuous stirred-tank reactor modeling approach considers all properties identical within the catalyst volume.

Chemical reactions take place on the surface of catalyst walls. Reactants have to diffuse sufficiently close to the catalyst wall to participate in the reactions. Ericson et al. in [52] modeled mass transfer from the gas to the catalyst surface by including two layers of channel walls. Another common approach is to consider each chemical specie in two forms: gas-phase and surface-type. Gas-phase species have to diffuse to the surface and only as the surface species can participate in reactions. Produced surface species subsequently diffuse back to the gas-phase [53–55]. But often, mass transfer between the bulk gas flowing through the catalyst and the surface is simplified as instantaneous [51,56], despite studies emphasizing its importance [23].

NH_3 storage mechanism Surface-type reactions in SCR catalyst require that one or more reactants adsorb to the surface. Two surface-type reaction mechanisms are used for SCR modeling: *Langmuir-Hinshelwood* mechanism assumes that two substances adsorb and consequently participate in the reactions [29], *Eley-Rideal* approach assumes that only one substance adsorbs on the surface. Most of the control-oriented approaches use Eley-Rideal mechanism and consider NH_3 the only specie to adsorb on the catalyst walls, where it participates in reactions with gas-phase NO_x.

NH_3 storage mechanism—the most important modeling feature included in every physics-based SCR model—comprises adsorption and desorption reactions. The amount of adsorbed ammonia is represented by a fraction θ (NH_3 coverage ratio) of a storage capacity of the channel. The storage capacity is modeled as a constant [57,58] or as a function of temperature [59,60].

Some authors argue that it is necessary to include two NH_3 storage sites to accurately describe the NH_3 storage mechanism. In [55] and [58] authors included second NH_3 storage site with smaller capacity: adsorbed NH_3 can leave it only through desorption, it does not participate in any chemical reactions. This allows the model to capture partial unavailability of the adsorbed NH_3 for NO_x reducing reactions.

Chemical reactions Set of reactions included in the model depends on aftertreatment configuration, catalytic washcoat formulation and required fidelity. For typical diesel engine exhaust gas NO_x concentrations, which comprise 70-90 % NO [24], NO_2 is often neglected and NO_x reduction is modeled by a standard reaction (3.2) only [51,61]. On the other hand, for configurations with upstream diesel oxidation catalyst or pre-oxidation catalyst—with NO_2/NO_x ratio around 0.5—three NO_x reducing reactions (3.2)–(3.4) are included in the model [34,56]. Formation of nitrous oxide (N_2O), oxidation of adsorbed NH_3 to nitrogen or NO can be included for models of catalysts with washcoat formulations sensitive to these unwanted reactions [62]. Chemical reaction rates are affected by concentrations of reactants and—as described by empirical Arrhenius formula—exponentially by temperature. Oxygen concentration is typically neglected in the model of standard reaction (3.2), where oxygen along with adsorbed NH_3 reduce NO, as it is considered always available for reaction. Various modeling approaches often differ in additional features introducing dependence of kinetic parameters on NH_3 coverage ratio and temperature.

Thermal model As discussed in Chapter 3, temperature plays an important role in the SCR catalyst. Thermal model—often an integral part of single-dimensional SCR models [55, 58, 61]—models heat transfer to predict axial temperature profile. Heat transfer modeled in the catalyst comprises heat conduction within the bulk-gas and the monolith, and heat convection due to flow of the gases. Further, thermal models can include: heat transfer between the bulk-gas and the monolith, heat transfer between the monolith and the catalyst housing, and heat transfer between the housing and the ambient. Reactions in the catalyst produce heat, but their impact is relatively small and for control-oriented models usually omitted [61].

Model identification Identification of model parameters is often performed on data obtained by using synthetic gas mixtures generated in a flow reactor. This approach allows for more variability in the gas composition, experiments can be designed to excite only a subset of phenomena and thus decouple the the complex behavior of the catalyst [55]. However, parameter identification from engine data allows to use more realistic gas composition [63].

Modeling studies A control-oriented zero-dimensional model by Upadhyay et al. [51]—used in many model-based estimator designs—considers four states: gas-phase NO_x, NH_3 and NH_3 coverage ratio θ. It neglects diffusion of gase-phase species to the surface and adopts Eley-Rideal reaction mechanism. Model accuracy can be improved by modeling NO_x separately as NO and NO_2 [56, 62]. However, NO, NO_2 and NH_3 concentration dynamics are often omitted: authors in [55,58,61] consider NH_3 coverage ratio θ and internal temperature as the only two states, and calculate outlet concentrations from algebraic equations. As the amount of literature published on SCR modeling is vast, Tab. 4.1 summarizes and compares several selected control-oriented models.

Reference	Axial elements	States	Purpose	Complexity
[63] Song et al., 2013	10	NO, NO_2, NH_3, θ_1, θ_2	estimation	nonlinear
[53] Na et al., 2011	15	θ, T	for control design	linearized
[34] Herman et al., 2009	12	NO, NO_2, NH_3, θ	feedback control	nonlinear
[64] McKinley, 2009	20	θ, T	feedback control	linearized
[52] Ericson et al., 2008	6	θ_1, θ_2, θ_3	real-time simulation	nonlinear
[61] Schär, 2003	13	θ, T	feedback control	linearized
[51] Upadhyay et al., 2002	1	NO_x, NH_3, θ	for control design	nonlinear

Table 4.1: SCR Modeling studies. Selected control-oriented SCR modeling studies.

4.2 Estimation

This section discusses estimation approaches that combine measurements of inputs and outputs with a physics-based model of the SCR catalyst to:

- provide estimates of unmeasurable physical quantities
- improve accuracy of the measurements
- replace physical sensors for cost reduction

Inspired by the reviewed literature, I identified the following requirements that estimators have to satisfy to provide information about the underlying process (not ranked):

1. Guaranteed stability under feasible operating conditions
2. Good steady-state and transient estimation performance
3. Robustness to modeling uncertainties and measurement error over wide range of ambient conditions, including low-temperature condition
4. Cost-effectiveness
5. Low computational complexity

Fig. 4.3 below shows the full physical sensor set for estimation of SCR, which comprises NO_x sensors, NH_3 sensors and thermocouples at the inlet and outlet of the catalyst [65]. Further information might be required by the estimators: exhaust mass flow, oxygen concentration and exhaust gas pressure can be obtained from existing engine-out measurements or calculations.

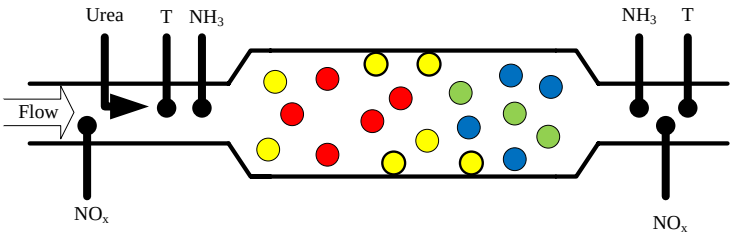

Figure 4.3: Full sensor set for estimation of SCR. The sensor set for estimation of SCR comprises NO_x sensors, NH_3 sensors and thermocouples at the inlet and outlet of the catalyst. NO_x at the inlet is measured upstream of urea injector to avoid corruption by sensor cross-sensitivity to NH_3 [65].

Estimation of NH_3 coverage ratio and outlet NO_x and NH_3 concentrations receive the most interest in the reviewed literature. Other topics of interest include cross-sensitivity of production NO_x sensors to NH_3, estimator robustness to model uncertainties and measurement error, and estimation with reduced physical sensor set. I discuss these in more detail in the following sections. Tab. 4.2 at the end of the chapter summarizes estimation approaches with respect to estimated variables.

4.2.1 Estimation of concentrations and NH_3 coverage ratio

I have identified several groups of SCR catalyst observer design approaches ranging from simple steady-state observers, including linear and nonlinear state observers, robust sliding mode designs, Kalman filter implementations and more advanced designs such as gain-scheduling proportional-multiple-integral (PMI) estimator. The following discussion, sorted by the design approach group, introduces estimation approaches published in literature with focus on the approach itself, the estimation goal, underlying model and sensor set used.

Steady-state estimation

Steady-state NH_3 coverage ratio estimators can be obtained by omitting either NH_3 coverage ratio dynamics [66], NH_3 outlet concentration dynamics [66] or NO_x dynamics [67]. In contrast to [66], the approach in [67] does not require full sensor set shown in Fig. 4.3; inlet and outlet NO_x concentrations provide sufficient information to estimate the NH_3 coverage ratio as a scheduling variable for proposed model-based control.

Steady-state observer in [68] utilizes NO and NO_2 estimates provided by Extended Kalman Filter and calculations from two outlet NO_x sensors to estimate NH_3 coverage ratio. Steady-state estimators are simple to implement and require low CPU resources, but are sensitive to model and measurement error [66] and—as pointed out in [69]—may hardly be used in automotive applications because of the highly transient engine operations.

Linear state observers

Nieuwstadt and Upadhyay designed a linear observer for NH_3 coverage ratio and NO_x and NH_3 outlet concentrations [70]:

$$\dot{\hat{x}} = f(\hat{x}, C_{\mathrm{NH_{3_{in}}}}, C_{\mathrm{NO_{x_{in}}}}) + L(\hat{C}_{\mathrm{NO_x}} - C_{\mathrm{NO_x}}) \tag{4.1}$$

where $\hat{x} = \left[\hat{C}_{\mathrm{NO_x}}, \hat{\theta}, \hat{C}_{\mathrm{NH_3}}\right]$ is the state estimate and f denotes a nonlinear model function. They do not choose optimal gains L for their observer nor does Devarakonda et al. in [62], where they proposed similar linear state observer for a 4-state model, which considers separate NO and NO_2 concentrations.

Sliding mode observers

Hsieh et al. [57] compared an observer based on NH_3 coverage ratio dynamics with two sliding mode observer designs for estimation of NH_3 coverage ratio. Sliding mode design based on NH_3 coverage ratio and NH_3 concentration dynamics, which requires outlet NH_3 sensor, was found to be robust to temperature and NO_x measurement errors. Sliding mode observer based on NH_3 coverage ratio and NO_x concentration dynamics, which does not require NH_3 sensor, was found sensitive. Recently, Chen et al. in [69] proposed sliding mode observer design claiming the observer's robustness to input uncertainties. The observer does not require NH_3 sensor. Other authors in [59] showed an application of sliding mode observer for a two SCR in-series setup for estimation of mid-catalyst NH_3 concentration. Zhang et al. [66] came up with smooth variable structure (SVS) observer and found it superior to sliding mode observers [57] in terms of robustness, estimation performance and computational demands; authors claim that the observer does not increase stiffness of the underlying model.

Extended Kalman filter

Kalman filter combines predictions of a linear model and noisy measurements in optimal manner to estimate the system states. Extended Kalman filter (EKF) is used for estimation of nonlinear systems. Hsieh et al. [71] used EKF to estimate NH_3 coverage ratio and NH_3 storage capacity M for potential OBD use; M is considered as slowly time-varying parameter and modeled as constant. Zhou et al. in [72] compared predictions of SCR model comprised of four axial elements with estimations by EKF based on single-element model. Surenahalli et al. [58] compared EKF estimates obtained with different outlet sensor configurations. Chen et al. [68] used EKF to estimate separately NO and NO_2 concentrations from outlet NO_x—after

correcting for NO_x sensor cross-sensitivity to NH_3—and used the estimates for further estimation of NH_3 coverage ratio by steady-state NH_3 coverage ratio estimator. EKF approach has been used in several studies to estimate NO_x concentrations from NO_x sensor cross-sensitive to NH_3 [71, 73]. More about the approach can be found in the discussion below.

Nonlinear Luenberger-like observers

McCarthy et al. [74] proposed a nonlinear switched observer using only NO_x sensor measurements, however Chen et al. [68] pointed out that implementing this observer in practice is questionable, since NO_x sensor cross-sensitivity to NH_3 is neglected. Zhang et al. [60] proposed a nonlinear state observer. Proportional gains were chosen, but not optimally computed, and the observer was shown stable by Lyapunov-based analysis. Authors employed this observer to estimate NH_3 coverage ratio and NH_3 concentration of downstream SCR catalyst in a two-catalyst setup [75].

High-gain observers

Chen et al. presented his approach to estimate inlet and outlet NH_3 concentration with a high-gain observer in [76]. At low temperatures, unconverted urea solution and an intermediate product of urea-NH_3 conversion, HNCO, may appear at the catalyst inlet and outlet. Since these species cannot be measured by NH_3 sensor, authors designed the observer to include their concentration into the NH_3 concentration estimates. Zhang et al. [77] use high-gain observer approach with inlet NO_x as well as outlet NO_x and NH_3 sensor measurements to estimate NH_3 input and NH_3 coverage ratio.

Proportional integral observer

Zhang et al. [75] introduced two proportional-integral (PI) observers for estimating NH_3 coverage ratio along with either NH_3 input or inlet NO_x where estimation of the latter is more accurate. NH_3 coverage ratio shows almost zero estimation error for both observers after initial settling. It converges faster when estimated along with inlet NO_x.

4.2.2 Estimation of NO_x sensor cross-sensitivity to NH_3

Production NO_x sensors lump measurements of NO, NO_2 and NH_3 concentrations together, which makes urea injection control based on NO_x sensor feedback less efficient and estimation of SCR inaccurate [78]. Authors in [65, 71, 78] combined SCR model and NO_x sensor model (4.2) to estimate outlet NOx concentrations C_{NO_x} and cross-sensitivity factor K_{cs}, which indicates how significantly NH_3 corrupts NO_x measurements. The estimation of this temperature-dependent factor is useful for malfunction checking and NO_x and NH_3 sensor aging monitoring [73].

$$C_{NO_{x,\,sensor}} = C_{NO_x} + K_{cs} C_{NH_3} \tag{4.2}$$

The EKF approach [71] based on 3-state model was further extended in [73] to provide separate NO and NO_2 concentrations estimates. However, adaptive urea control law with adaptive-network-based fuzzy inference system (ANFIS) by Wang et al. [79] outperforms control law with EKF estimates from [73] by 58.64 % and 20.6 % over an US06 test cycle in terms of 2-norm and ∞-norm of NO_x concentration error respectively.

In robust gain-scheduling observer designs [65] and [78] authors consider K_{cs} bounded in first and q-th derivative, respectively; increasing q lowers estimation error at the cost of increased computational load. In reference [65], EKF from [71] is found considerably slower and its

performance inferior to the proposed observer. Chen et al. [68] use two outlet NO_x sensors modeled by eq. (4.2)—each with distinct temperature-dependent cross-sensitivity behavior in the operating temperature range—to estimate NO_x and NH_3 concentration without requiring NH_3 sensor.

4.2.3 Estimation accuracy and robustness

Cross-sensitivity of production NO_x sensor to NH_3 is not the only source of estimation error. Estimation accuracy can be negatively affected by input uncertainty and quality of the underlying model. SCR model accuracy depends on the considered set of chemical reactions and the effort put into calibration of the reaction rate kinetic parameters. Further, number of axial elements used to describe the catalyst has significant effect on model accuracy; Herman et al. [34] compared NO_x and NH_3 concentration prediction error of control-oriented models with 4-16 axial elements. SCR estimators robust to input uncertainties were proposed only recently. Chen et al. [76] claim to be the first to propose an observer robust to incomplete decomposition of urea to NH_3 exhibited at low-temperatures, their observer also estimates inlet NH_3 concentrations. Robust input estimators were further proposed in [75, 77]. Approach in [69] is claimed robust to input uncertainty, but inputs are not estimated.

Authors of the reviewed literature rarely publish statistical properties of the estimation error. From the papers summarized in Tab. 4.2 only [58] and [72] provide maximum or mean error of NO_x and NH_3 outlet concentrations and its standard deviation. Estimation accuracy in the reviewed literature is discussed in terms of how well the estimates track or how fast they converge to either measured values or to values obtained by simulating models calibrated to physical SCR catalyst.

Since NH_3 storage is not measurable, estimated values can be only compared to simulated model predictions, which might not reflect the true NH_3 storage in the catalyst. Authors in [66, 68] proposed estimators robust to uncertainty in model parameters, they claim that estimated NH_3 coverage and outlet specie concentrations are more accurate than the model predictions.

Temperature significantly affects sources of uncertainties: incomplete urea to NH_3 conversion is exhibited at low-temperatures; exponential temperature dependence of chemical reaction rates makes the estimates more sensitive to model uncertainties [51]; and NO_x sensor cross-sensitivity factor K_{cs} as given in eq. (4.2) is also strongly temperature dependent [79].

4.2.4 Substituting physical sensors with estimates

Estimating variables rather than measuring them with expensive physical sensors is one of the key motivators for development of estimators (virtual sensors). Reduction of the set of physical sensors used in SCR aftertreatment setup has recently gained more attention in the literature. Inlet NO_x sensor, from the full sensor set shown in Fig. 4.3, can be substituted by engine-out maps [77], engine-out or pre-SCR virtual NO_x sensors [58], or estimated using a SCR model-based approach [75]. Inlet NH_3 can be computed from measured exhaust flow and urea injector data [60]. However, this might be inaccurate due to incomplete urea to NH_3 conversion, especially at low temperatures. Estimators of inlet NH_3 were proposed in [75–77]. Outlet NH_3 sensor offers several advantages for feedback control of urea injection. For example, it corrects NO_x sensor cross-sensitivity to NH_3 and allows for lower NH_3 slip compared to control based on NO_x sensor only. This made outlet NH_3 a sensor of choice in many SCR control studies [34, 54, 80, 81]. However, NH_3 sensor still remains too costly for production [69], and thus control [67, 82, 83] and estimation approaches [60, 68, 69] that refrain from using NH_3 sensors were published recently.

4.2.5 Processor load and memory

On-ECU implementation and CPU and memory requirements specifically for estimation of SCR are not sufficiently discussed in the reviewed literature. I found several publications, where these aspects are discussed with respect to entire control algorithm, which includes model-based estimation. Herman et al. [34] proposed a control approach based on control-oriented model, which involves NH_3 storage estimation. They claim that the proposed approach has been successfully implemented in a single-precision floating point embedded microprocessor. McKinley [37, 84] designed model predictive control and Chen et al. [85] nonlinear model predictive control for urea injection.

Research team from Delphi introduced a model-based closed-loop control approach with NH_3 sensor included for aftertreatment configuration comprising SCR/DPF and under-floor SCR [86]. They claim that their NH_3 coverage observer can run on ECU, but only few details are provided about the implementation. Similarly, AVL proposed a control approach with state-estimation, which they claim suitable for on-ECU implementation [50]. SCR is a stiff system since the adsorption and desorption of NH_3 are much faster processes than NH_3 consumption. Stiff systems require faster sampling rate and thus increase computational load. Zhang et al. [66] claim that their smooth variable structure observer does not increase the stiffness of the underlying model and that it performs better than sliding mode observers [57], it is more robust and comes with lower CPU requirements. Further Zhang et al. [65] proposed a gain-scheduling observer for NO_x outlet estimation from NO_x sensor cross-sensitive to NH_3, which uses less CPU resources and outperforms EKF approach from [71].

Estimated variable	Position	References
NH_3 coverage ratio	internal	[70], [62], [57], [71], [59], [67], [72], [74], [58], [66], [76], [75], [68], [69], [77].
NH_3 concentration	internal	[59], [74], [58].
	outlet	[70], [62], [57], [72], [74], [66], [76], [60], [75], [68], [69].
	inlet	[76], [75], [77].
NO_x concentration	internal	[74].
	outlet	[70], [57], [71], [74], [76] [60], [75], [69], [65], [78].
	inlet	[75].
NO and NO_2 concentration	internal	[58].
	outlet	[62], [73], [72], [68].
Temperature profile	internal	[58].
NO_x sensor cross-sensitivity	outlet	[71], [73], [65], [78].
NH_3 storage capacity M	internal	[71].

Table 4.2: Estimated states and parameters. Summary of the reviewed estimation approaches sorted with respect to estimated states and parameters.

Chapter 5

Development of SCR catalyst model

This chapter discusses development of a nonlinear physics-based SCR catalyst model for a model-based SCR estimator. Section 5.1 introduces the aftertreatment configuration and the modeling problem. Section 5.2, which was in a preliminary form previously published in [87], describes modeling of gas flow in the catalyst and discusses effects of flow-channel discretization on model accuracy. The following section 5.3 discusses modeling of chemical reactions, and sections 5.4 and 5.5 propose two lower-fidelity models: the *5-state lower-fidelity model* and the *2-state lower-fidelity model*. Section 5.6 describes the design of experiment for a 6-phase parameter identification procedure. Finally, section 5.7 analyzes performance of the proposed lower-fidelity models in simulations.

5.1 Modeling problem

The modeling problem for the purpose of this thesis includes design and calibration of a lower-fidelity model that captures main phenomena of SCR catalyst and allows for fast simulation as a part of a SCR estimator. The modeled SCR catalyst features in aftertreatment system for light-duty diesel-engine application, which comprises a cascade of three devices: Diesel Oxidation Catalyst (DOC) downstream of the engine, followed by SCR and ammonia oxidation catalyst (AMOX). Fig. 5.1 below shows the aftertreatment configuration.

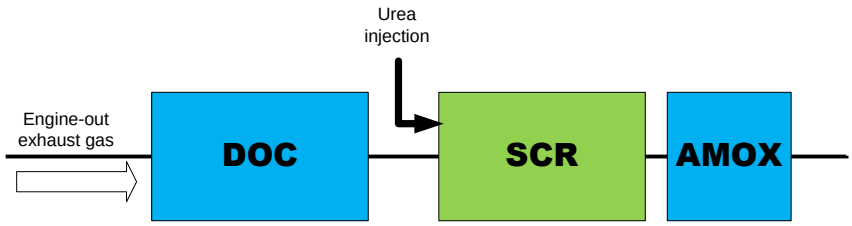

Figure 5.1: Configuration of aftertreatment. Diesel Oxidation Catalyst (DOC) is followed by a Selective Catalytic Reduction (SCR) catalyst and ammonia oxidation catalyst (AMOX).

Simulations of a high-fidelity model of the complete aftertreatment system—calibrated from engine and aftertreatment experiment data—provided experimental data for calibration of two proposed lower-fidelity models. For the calibration process, I disabled the upstream DOC in the high-fidelity model to get full control over SCR inlet species' concentrations and used the measurements directly downstream of the SCR to exclude interference from the AMOX catalyst.

I could affect the behavior of the high-fidelity model by adjusting parameters of modeled features on its interface, but I was unable to see its internal structure or any specific details about

its implementation. However, the reaction rate parameters shown on the interface of the high-fidelity model helped me select the set of chemical reactions to include in my lower-fidelity models.

5.2 Channel model

Partial differential equation (5.1) is a sufficiently accurate description of gas flow through a catalyst approximated by single-dimensional channel. It describes transfer of a single chemical specie expressed in concentrations C with a flow velocity v along the channel length in the x dimension. The equation comes from the general description of fluid motion—Navier-Stokes equations—by assuming non-viscous flow of incompressible gases with constant flow velocity [88]. It includes effects of chemical reactions—with diffusion of the bulk-gas to the catalyst surface omitted—through the source term S_r:

$$\frac{\partial C}{\partial t} + v\frac{\partial C}{\partial x} = S_\mathrm{r} \tag{5.1}$$

Flow-channel discretization

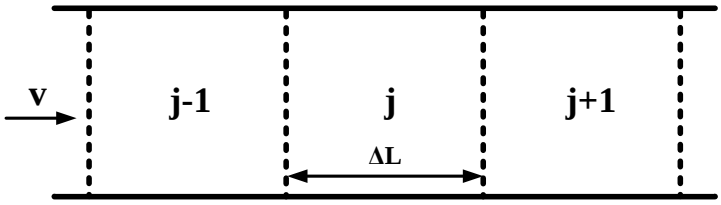

Figure 5.2: Flow-channel discretization. Single-channel approximation of SCR catalyst discretized to axial elements for numerical methods in eq. (5.2)–(5.5).

Finite-difference numerical methods for solving partial differential equations (PDE) approximate the partial derivatives with finite-differences. In other words, they discretize the domain to finite number of elements. In the following paragraphs I compare accuracy of three finite-difference schemes applied on single-channel catalyst model from (5.1) with inactive chemical reactions. The methods discretize the PDE both in time and space, denoted by superscript n and subscript j; $\alpha = v\Delta t/\Delta L$, where Δt denotes sampling time and ΔL axial element length:

A) **1st-order-accurate scheme in time and space**

$$C_j^{n+1} = C_j^n - \alpha\left(C_j^n - C_{j-1}^n\right) \tag{5.2}$$

This scheme is also called *donor cell method* or *upwind method* [89].

B) **2nd-order-accurate scheme in time and space**

$$C_j^{n+1} = C_j^n + \alpha\left(-C_j^n + C_{j-1}^n\right) + \frac{\alpha}{2}\left(-\Delta C_j^n + \Delta C_{j-1}^n\right) + \frac{\alpha^2}{2}\left(\Delta C_j^n - \Delta C_{j-1}^n\right) \tag{5.3}$$

The undivided differences ΔC_j^n denote concentration differences between neighboring elements disregarding the element size [90]. Three fundamental ways to define these differences—backward, forward and central—make up Beam-Warming, Lax-Wendroff

and Fromm schemes after substituting into (5.3). Fig. 5.3 compares the other two methods with Lax-Wendroff scheme that uses forward undivided differences:

$$\begin{aligned} \Delta C_j^n &= C_{j+1}^n - C_j^n \\ \Delta C_{j-1}^n &= C_j^n - C_{j-1}^n \end{aligned} \tag{5.4}$$

***C*) 2nd-order-accurate model in time and space with non-linear flow limiter**
According to Godunov's theorem [89], linear methods can produce monotonicity-preserving scheme only up to first order accuracy. Monotonicity is an important property since non-monotonic discretization schemes introduce unwanted oscillations, and they can make a positive-value problem take up negative values, which introduces problems for flow channel modeling. As a consequence of Godunov's theorem, any linear 2nd-order-accurate scheme is non-monotonic. Implementing nonlinear limiters—such as MC limiter in eq. (5.5)—guarantees monotonicity:

$$\begin{aligned} \Delta C_j^n = \frac{1}{2}\Big(&\text{sign}(C_{j+1}^n - C_j^n) \\ &+ \text{sign}(C_j^n - C_{j-1}^n)\Big) \min\left(\frac{1}{2}|C_{j+1}^n - C_{j-1}^n|, 2|C_{j+1}^n - C_j^n|, 2|C_j^n - C_{j-1}^n|\right). \end{aligned} \tag{5.5}$$

Fig. 5.3 shows propagation of two rectangular peaks in NO_x concentration through a single-dimensional channel discretized to $N = 101$ elements for the different discretization schemes. The finite-difference schemes introduce dissipation, amplitude loss, oscillation and negative concentration values. Only the 2nd-order-accurate scheme with nonlinear limiter (5.5) gives reasonable approximation to the partial differential equation.

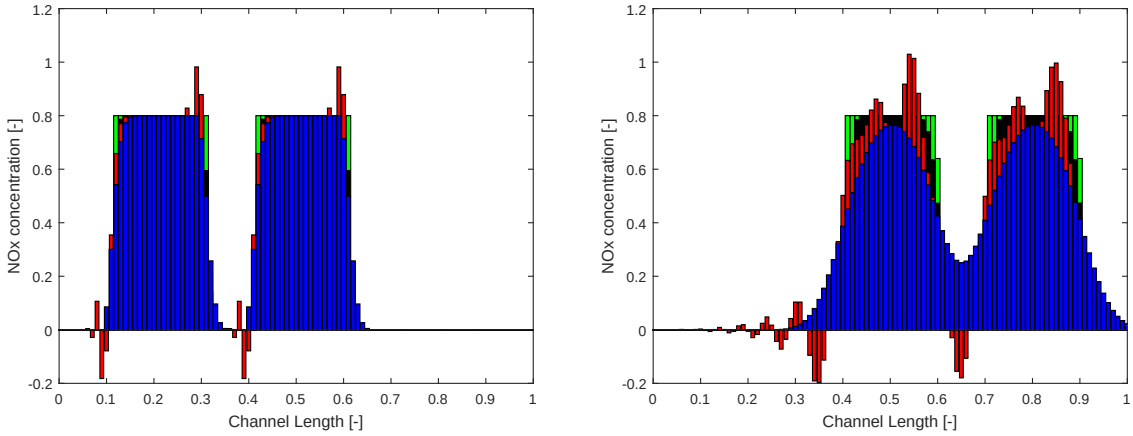

(a) **(b)**

Figure 5.3: Propagation of gases through the catalyst. Two rectangular peaks in NO_x concentration propagate through a single-dimensional channel with a constant velocity. There are no chemical reactions taking place. Fig. a) shows the concentration profiles in the channel shortly after initial time. Fig. b) shows that as the gas propagates the finite-difference schemes introduce dissipation, amplitude loss, oscillation and negative concentration values. Green denotes the ideal concentration profile, the methods *A*, *B* and *C* are denoted by blue, red and black color.

However, for fewer axial elements, $N < 30$, the difference in accuracy between the higher-order nonlinear methods and the simplest first order upwind method is much smaller than for the case with $N = 101$ presented above. Consequently, I decided to propose a lower-fidelity model that uses the least computationally demanding scheme *A* (5.2) for a channel approximated by a single element only.

5.3 Chemical reactions

The source term S_r on the right hand side of eq. (5.1) can be expressed as a sum of rates of all chemical reactions in which the chemical specie participates:

$$\frac{\partial c}{\partial t} + v\frac{\partial c}{\partial x} = \sum_i \sigma_i r_i, \tag{5.6}$$

Stoichiometric coefficients σ_i denote the number of molecules participating in the reactions. Rates of chemical reactions r_i depend on concentrations of reactants, and temperature T. Arrhenius law introduces kinetic parameters A_i (pre-exponential coefficient) and E_i (activation energy) to describe the exponential temperature-dependence, R denotes the gas constant:

$$r_i = A_i e^{\frac{E_i}{RT}} \prod_j C_j. \tag{5.7}$$

The model uses Eley-Rideal surface-type reaction mechanism, which assumes adsorption of NH_3 on the catalyst walls. The proposed model includes two NH_3 storage sites. Concentration of the stored NH_3 on each of the sites, denoted $C_{NH_3^*}$ and $C_{NH_3^{**}}$, can be expressed as a NH_3 coverage ratio $\theta_i \in \langle 0, 1\rangle$ of NH_3 storage capacity M_i, where i denotes ith site:

$$C_{NH_3^*} = \theta_1 M_1. \tag{5.8}$$

$$C_{NH_3^{**}} = \theta_2 M_2. \tag{5.9}$$

The model further features concentrations of gas-phase NO, NO_2, NH_3, and eight chemical reactions: adsorption and desorption reaction for each of the two NH_3 storage sites; standard, fast and slow NO_x reducing reactions; and oxidation of adsorbed NH_3. I excluded the reaction products—water (H_2O) and nitrogen (N_2)—from the model, since the reactions have negligible effect on their concentrations in the exhaust gas. I assume oxygen as always available for standard reaction by considering the reaction rate oxygen-independent, since its concentrations in the exhaust gas are much higher than concentrations of the other reactants, NO and NH_3^*. In contrast, oxygen concentration features in the NH_3 oxidation reaction model. Tab. 5.1 summarizes included reactions.

Reaction	Chemical equation	Reaction rate
Site 1 NH_3 storage	$NH_3 + S_1 \longleftrightarrow NH_3^*$	$r_{ads_1} = k_{ads_1} C_{NH_3}(1-\theta_1) M_1$ $r_{des_1} = k_{des_1}\theta_1 M_1$
Site 2 NH_3 storage	$NH_3 + S_2 \longleftrightarrow NH_3^{**}$	$r_{ads_2} = k_{ads_2} C_{NH_3}(1-\theta_2) M_2$ $r_{des_2} = k_{des_2}\theta_2 M_2$
Standard	$4NH_3^* + 4NO + O_2 \longrightarrow 4N_2 + 6H_2O$	$r_{std} = k_{std} C_{NO}\theta_1 M_1$
Fast	$2NH_3^* + NO + NO_2 \longrightarrow 2N_2 + 3H_2O$	$r_{fast} = k_{fast} C_{NO} C_{NO_2}\theta_1 M_1$
Slow	$8NH_3^* + 6NO_2 \longrightarrow 7N_2 + 12H_2O$	$r_{slow} = k_{slow} C_{NO_2}\theta_1 M_1$
NH_3 oxidation	$4NH_3^* + 3O_2 \longrightarrow 2N_2 + 6H_2O$	$r_{oxi} = k_{oxi} C_{O_{2in}}\theta_1 M_1$
$k_i = A_i e^{\frac{E_i}{RT}}$ for $i = ads_1, ads_2, des_1, des_2$, std, fast, slow, oxi		

Table 5.1: Modeled chemical reactions.

5.4 5-state lower-fidelity model formulation

The proposed nonlinear *5-state lower-fidelity model* of SCR catalyst considers single axial element of length L and comprises:

- states – concentrations of NO, NO_2, NH_3, and NH_3 coverage ratios of 1st and 2nd site: C_{NO}, C_{NO_2}, C_{NH_3}, θ_1, θ_2
- inputs – inlet concentrations of NO, NO_2, NH_3, O_2, temperature, exhaust gas, mass flow and inlet pressure: $C_{NO_{in}}$,$C_{NO_{2in}}$, $C_{NH_{3in}}$, $C_{O_{2in}}$, T, $\dot{m}$, P_{in}

I assume all concentrations in mol/m^3. Ideal gas law is used for unit conversion of inlet specie concentrations from ppm to mol/m^3:

$$C = \frac{P_{in}}{10^6 RT} C^{ppm}. \tag{5.10}$$

The following set of ordinary differential equations describes the model (Tab. 5.1 summarizes the reaction rates r_i):

$$\frac{\partial C_{NO}}{\partial t} = -\frac{v}{L}\left(C_{NO} - C_{NO_{in}}\right) - 2r_{std} - r_{fast}, \tag{5.11}$$

$$\frac{\partial C_{NO_2}}{\partial t} = -\frac{v}{L}\left(C_{NO_2} - C_{NO_{2in}}\right) - 6r_{slow} - r_{fast}, \tag{5.12}$$

$$\frac{\partial C_{NH_3}}{\partial t} = -\frac{v}{L}\left(C_{NH_3} - C_{NH_{3in}}\right) - r_{ads_1} + r_{des_1} - r_{ads_2} + r_{des_2}, \tag{5.13}$$

$$\frac{\partial \theta_1}{\partial t} = \frac{1}{M_1}\left(r_{ads_1} - r_{des_1} - 2r_{std} - 8r_{slow} - 2r_{fast} - 4r_{oxi}\right), \tag{5.14}$$

$$\frac{\partial \theta_2}{\partial t} = \frac{1}{M_2}\left(r_{ads_2} - r_{des_2}\right) \tag{5.15}$$

Exhaust gas flow velocity v is computed from mass flow $\dot{m}$, frontal flow area of the catalyst A_f and exhaust gas density ρ:

$$v = \frac{\dot{m}}{A_f \rho}. \tag{5.16}$$

Ideal gas law gives exhaust gas density:

$$\rho = \frac{P_{in}}{M_{gas}} RT, \tag{5.17}$$

where M_{gas} and R denote molar mass of exhaust gas and the gas constant, respectively.
I implemented the model in MATLAB as a right-hand-side function that can be used in arbitrary continuous-time numerical solver.

5.5 2-state lower-fidelity model formulation

I simplified the *5-state lower-fidelity model* by omitting dynamics in NO, NO_2 and NH_3 concentrations (5.11)– (5.13). The proposed nonlinear *2-state lower-fidelity model* comprises:

- states – NH_3 coverage ratios of 1st and 2nd site: θ_1, θ_2
- algebraic variables – concentrations of NO, NO_2, NH_3: C_{NO}, C_{NO_2}, C_{NH_3}
- inputs – inlet concentrations of NO, NO_2, NH_3, O_2, temperature, exhaust gas, mass flow and inlet pressure: $C_{NO_{in}}$, $C_{NO_{2in}}$, $C_{NH_{3in}}$, $C_{O_{2in}}$, T, $\dot{m}$, P_{in}

The following set of ordinary differential equations describes the *2-state lower-fidelity model*:

$$\frac{\partial \theta_1}{\partial t} = \frac{1}{M_1}\left(r_{\text{ads}_1} - r_{\text{des}_1} - 2r_{\text{std}} - 8r_{\text{slow}} - 2r_{\text{fast}} - 4r_{\text{oxi}}\right), \tag{5.18}$$

$$\frac{\partial \theta_2}{\partial t} = \frac{1}{M_2}\left(r_{\text{ads}_2} - r_{\text{des}_2}\right) \tag{5.19}$$

$$0 = -\frac{\nu}{L}\left(C_{\text{NO}} - C_{\text{NO}_{\text{in}}}\right) - 2r_{\text{std}} - r_{\text{fast}}, \tag{5.20}$$

$$0 = -\frac{\nu}{L}\left(C_{\text{NO}_2} - C_{\text{NO}_{2\text{in}}}\right) - 6r_{\text{slow}} - r_{\text{fast}}, \tag{5.21}$$

$$0 = -\frac{\nu}{L}\left(C_{\text{NH}_3} - C_{\text{NH}_{3\text{in}}}\right) - r_{\text{ads}_1} + r_{\text{des}_1} - r_{\text{ads}_2} + r_{\text{des}_2}, \tag{5.22}$$

Reaction rates r_i (Tab. 5.1), calculation of exhaust gas velocity (5.16), unit conversion of inlet concentrations (5.10) are identical as for *5-state lower-fidelity model*.

5.6 Identification

High-fidelity SCR model provided experimental data for identification of lower-fidelity models' parameters. It allowed excluding arbitrary reaction from the set of active reactions and consequently made it possible to design a 6-phase identification procedure where parts of the model could be identified separately from each other. Tab. 5.2 below summarizes the identification procedure. It shows activated parts of the model, parameters for identification and data used by the cost-function (5.24) in each identification phase.

Phase	**1st site**					**2nd site**	**Parameters Ω**	**Data**
	Ads/Des	Stand.	Slow	Fast	NH_3 ox.	Ads/Des		
1	×	×	×	×	×	✓	A_{ads_2}, A_{des_2}, E_{des_2}, M_2	NH_3, θ_2
2	✓	×	×	×	×	×	A_{ads_1}, A_{des_1}, E_{des_1}, M_1	NH_3, θ_1
3	✓	×	×	×	✓	×	A_{oxi}, E_{oxi}	NH_3
4	✓	✓	×	×	×	×	A_{std}, E_{std}	NO, NH_3
5	✓	×	✓	×	×	×	A_{slow}, E_{slow}	NO_2, NH_3
6	✓	×	×	✓	×	×	A_{fast}, E_{fast}	NO, NO_2, NH_3

Table 5.2: Design of experiment for model identification. It shows active reactions and parameters to be identified for each phase of identification procedure. High-fidelity model, used as a source of experimental data, allowed for enabling and disabling reactions.

I formulated the parameter identification as a nonlinear least-squares optimization problem of the following form:

$$\Omega^* = \underset{\Omega}{\text{argmin}} \, ||J(\Omega)||_2^2 \tag{5.23}$$

$$J(\Omega) = \sum_{\forall d \in \text{D}} a_d |d_{\text{meas}} - d_{\text{sim}}(\Omega)| \tag{5.24}$$

where a_d denotes manually tuned weighting and scaling parameters, and D is subset of selected data for particular identification phase as specified in Tab 5.2, it can comprise outlet NO, NO_2, NH_3 and internal θ_1, θ_2.

I performed the identification procedure in MATLAB: I simulated the *5-state lower-fidelity model* with variable-step size solver `ode15s` and used the native nonlinear least-squares solver

`lsqnonlin` with *trust-region-reflective* algorithm, which allows to specify bounds on parameters.

The first two phases serve for identification of the most important part of the model, NH_3 storage mechanism. For each NH_3 storage site there are 4 unknown parameters, i.e pre-exponential coefficients A_{ads} and A_{des}, desorption activation energy E_{des} and NH_3 storage capacity M. To simplify the identification, I considered adsorption reactions temperature-independent by setting their activation energies to zero, i.e. $E_{ads_1} = E_{ads_2} = 0$, similarly to models in [53], [55]. It turned out that NH_3 storage mechanism is best identified from steps in temperature with zero NO_x and constant NH_3 at the inlet.

NH_3 oxidation reaction rate depends on oxygen concentration in the exhaust gas. The identification experiments comprise constant inlet NH_3 and steps in O_2 concentration. I repeated the experiments for several temperatures held constant for the duration of the experiment. It was not necessary to cover the whole temperature operating range of the catalyst as NH_3 oxidation exhibits only at higher temperatures.

In contrast, experiments for identification of NO_x reducing reactions covered the whole temperature operating range, I let it increase with time from 200 to 445 °C. I kept inlet NO and NO_2 constant and chose similar sequence of inlet NH_3 concentration steps for identification of all three NO_x reducing reactions. Since fast reaction consumes both NO and NO_2, I identified the parameters from multiple datasets with NO_2/NO_x ratios 0.25, 0.5 and 0.75.

I repeated the above described experiments for several exhaust mass flow values from the operating range 10-70 g/s. It turned out that the identification procedure is insensitive to mass flow as the values of identified kinetic parameters, obtained from dataset with different mass flow, were similar.

Fig. 5.4–5.9 show one identification dataset for each of the six identification phases and compare the high-fidelity and lower-fidelity model predictions. Note that I had full control only over engine-out temperature, mass flow and gas concentrations; inlet pressure and the internal SCR temperature that serve as inputs for the lower fidelity models were provided by the high-fidelity model as measurements. Obliged by a confidentiality agreement, I omitted values of the identified parameters from the text.

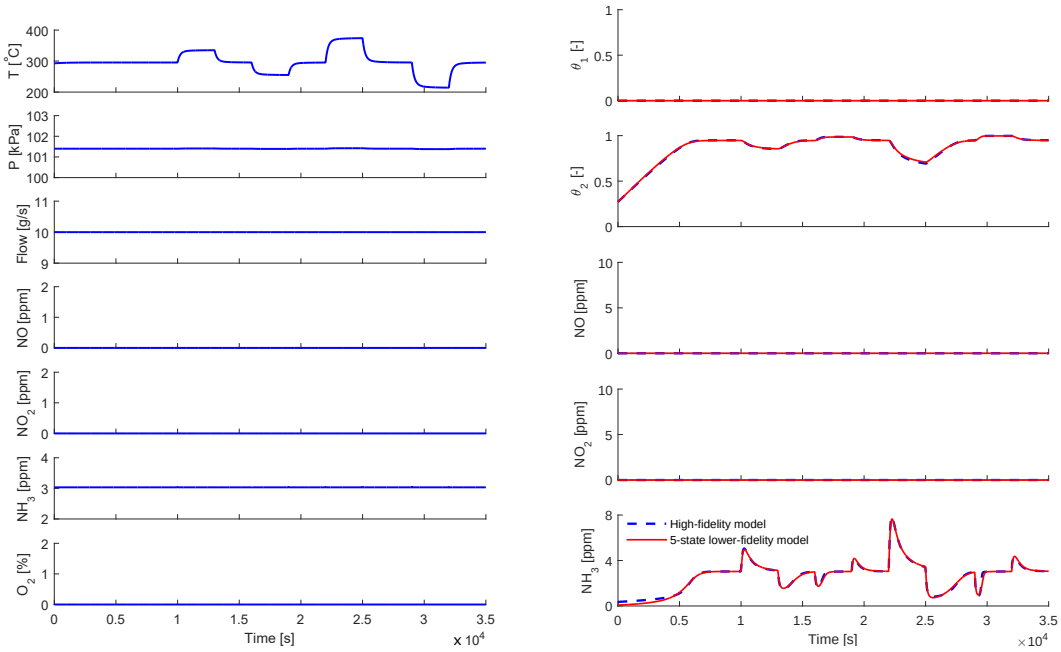

(a) inputs **(b)** outputs

Figure 5.4: Phase 1. Identification of NH_3 storage mechanism at 2nd site (Tab. 5.2).

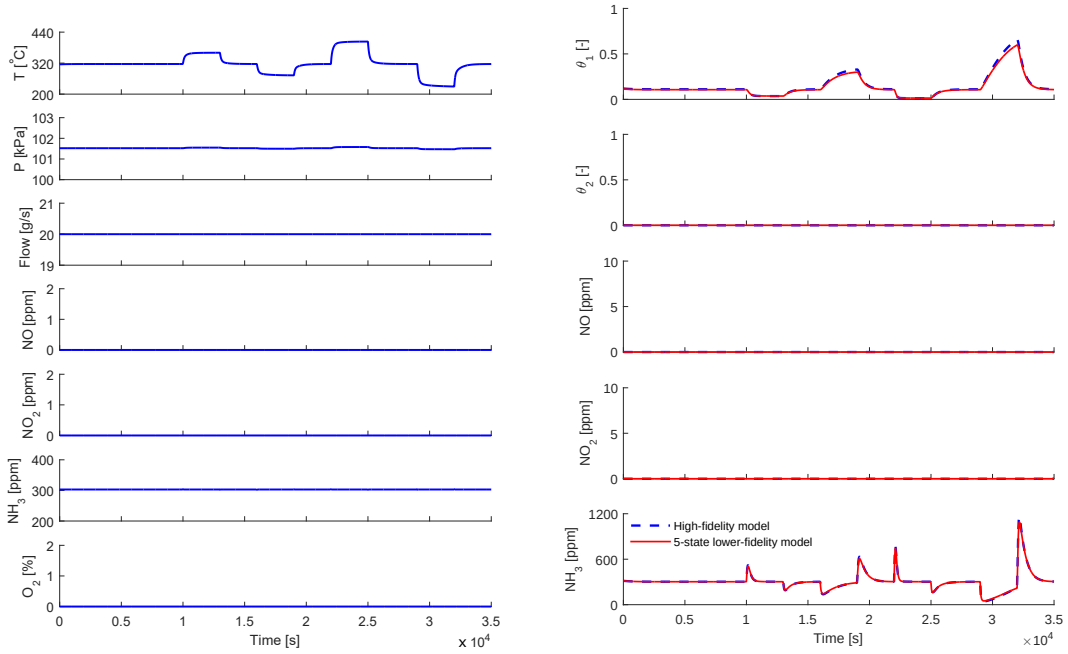

(a) inputs **(b)** outputs

Figure 5.5: Phase 2. Identification of NH_3 storage mechanism at 1st site (Tab. 5.2).

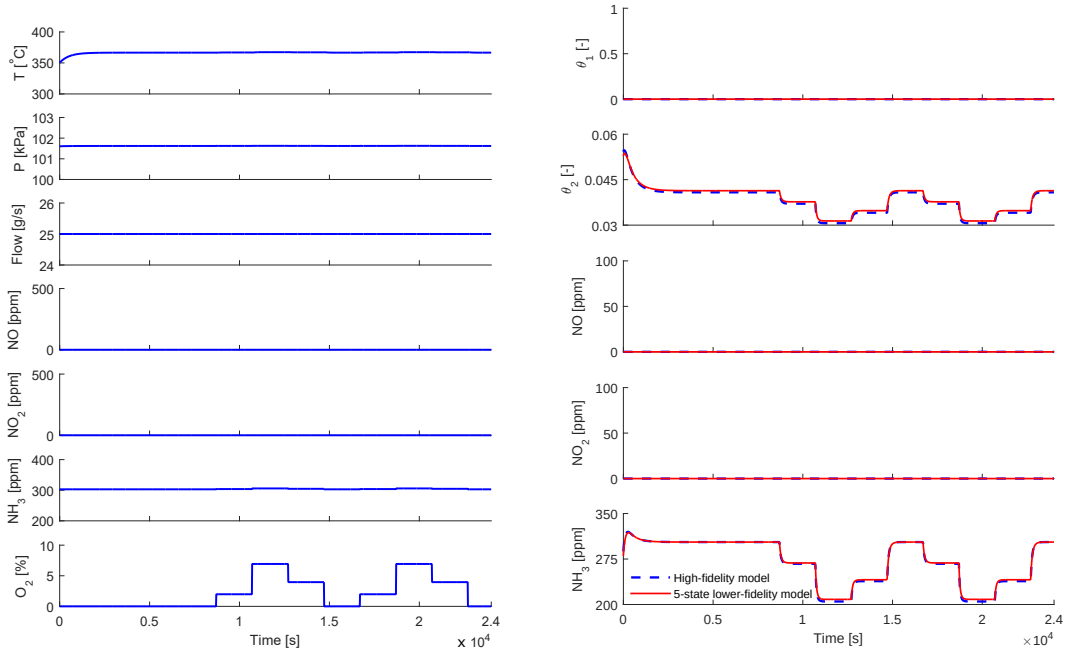

(a) inputs **(b)** outputs

Figure 5.6: Phase 3. Identification of oxidation of stored NH_3 on 1st site (Tab. 5.2).

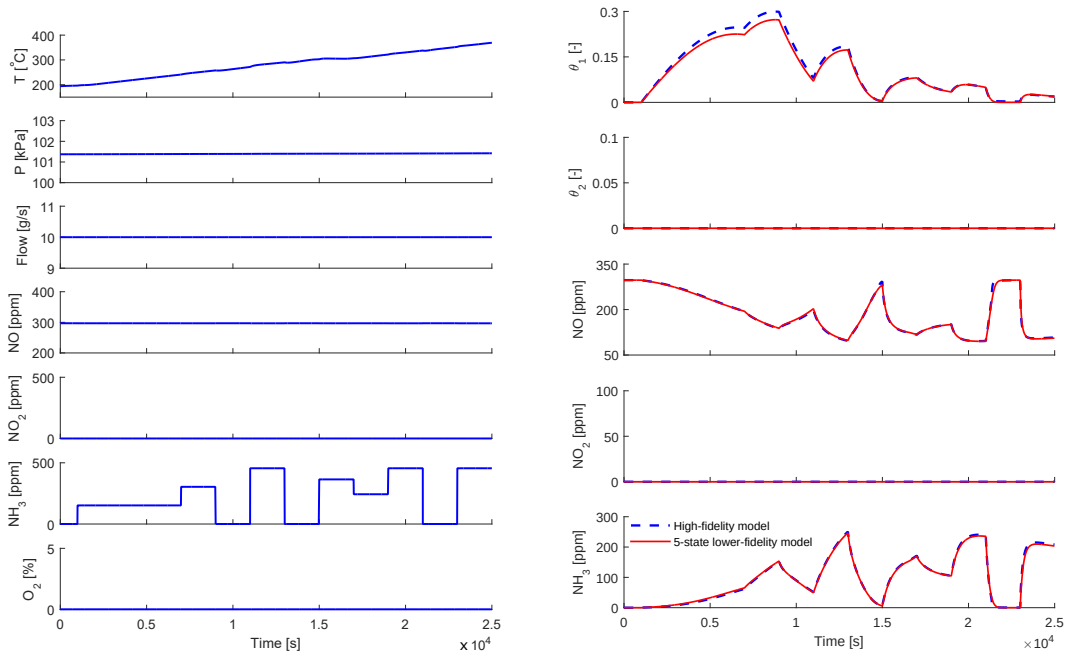

(a) inputs **(b)** outputs

Figure 5.7: Phase 4. Identification of standard reaction (Tab. 5.2).

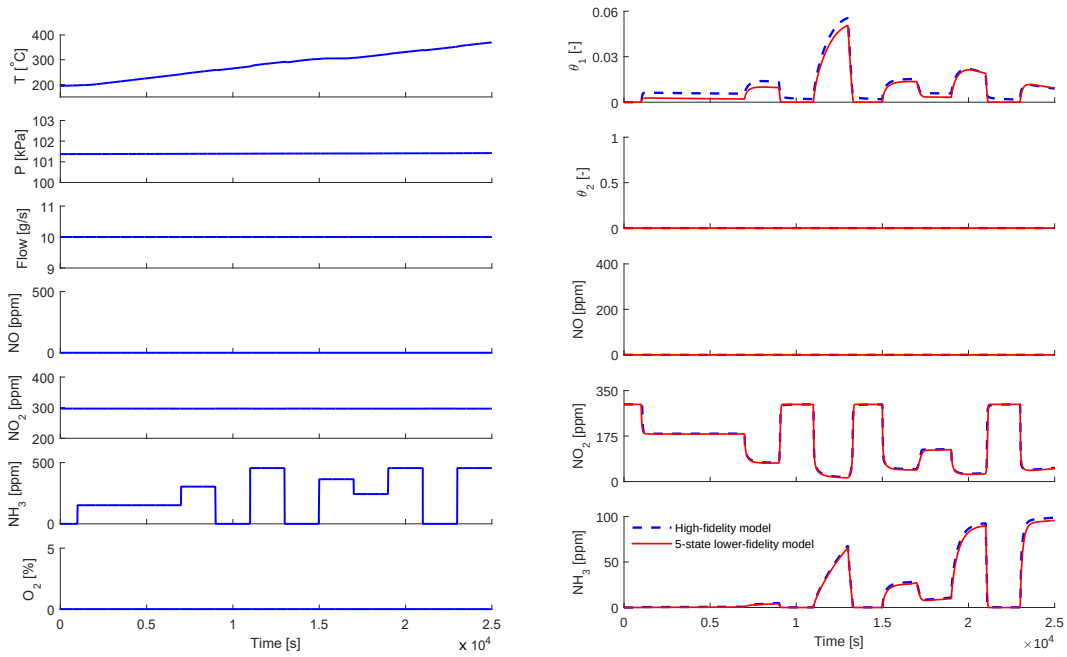

(a) inputs **(b)** outputs

Figure 5.8: Phase 5. Identification of slow reaction (Tab. 5.2).

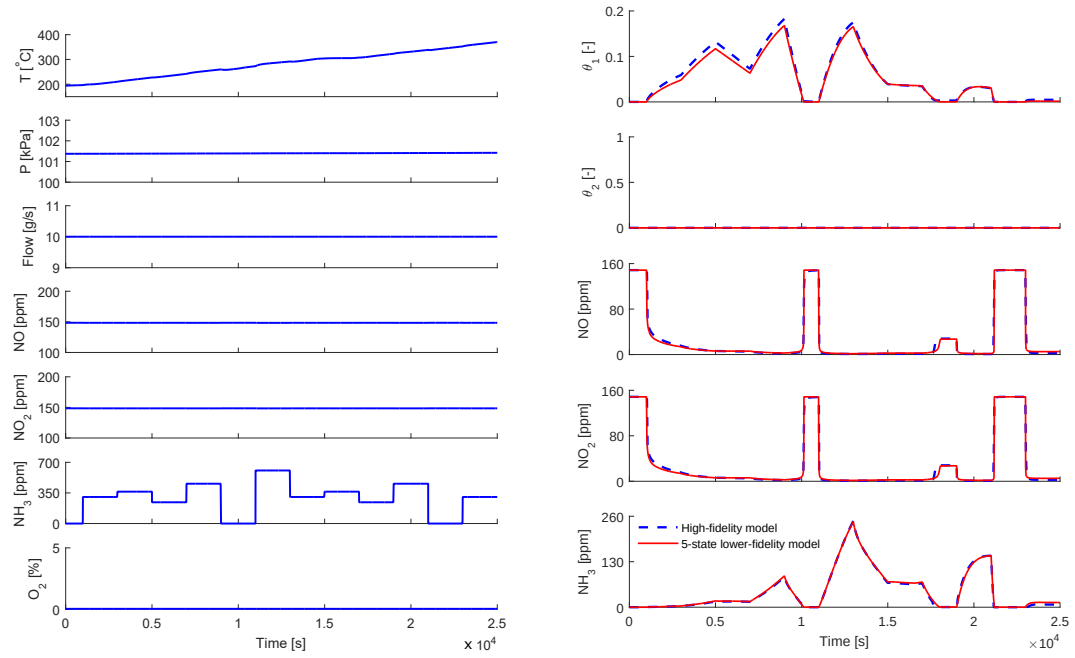

(a) inputs **(b)** outputs

Figure 5.9: Phase 6. Identification of fast reaction (Tab. 5.2).

5.7 Simulations and discussion

I originally proposed a 4-state nonlinear model which included dynamics in NO, NO_2 and NH_3 concentrations together with only one NH_3 storage site dynamics. I identified this model using phases 2–6 of the procedure described in section 5.6 to find out that the model performs well under operating conditions where sufficiently high amount of NH_3 is adsorbed on the catalyst walls. However, the 4-state model failed to produce results comparable to the high-fidelity model for lower NH_3 storage levels, where the SCR catalysts are normally operated to prevent undesired NH_3 slip during temperature transients.

To improve accuracy of the lower-fidelity model for operation at lower NH_3 storage levels I included a second NH_3 storage site (I discuss the justification for inclusion of second NH_3 storage site in literature review in Chapter 4). Open-loop simulation results of the *5-state lower-fidelity model* prove that it is an accurate approximation of the high-fidelity model. However, it does not satisfy the requirements for simulation on in-vehicle hardware: when simulated with a basic Forward Euler numerical integration method it requires sampling time of $\sim$10 µs in order to provide stable and sufficiently accurate predictions, which makes the model too slow for practical use. MATLAB simulation on a PC running Windows 7 with quad-core 2.8 GHz CPU, 8GB RAM and SSD drive was approximately 5× slower than real-time. More complex numerical integration methods, i.e. implicit or higher order schemes, might allow for larger sampling times and faster simulation at the cost of increased implementation complexity. Rather than implementing a different numerical integration method I simplified the model by omitting NO, NO_2 and NH_3 concentrations dynamics to obtain a non-stiff *2-state lower-fidelity model*, which allows for much faster sampling time $\sim 0.1s$ with Forward Euler method (I discuss this method in more detail in the following Chapter 6).

Diesel engine model calibrated in Honeywell's ONRAMP DESIGN SUITE provided engine-out data for the high-fidelity aftertreatment model. I simulated the engine over a WLTC Class

3 light-duty driving cycle [91]. High-fidelity aftertreatment model provided measurements upstream of the SCR catalyst as inputs for the proposed lower-fidelity SCR models. Urea injection was initiated at 399 s and kept to maintain $NH_3/NO_x = 1$ between 450-1500 s. Fig. 5.10 compares open-loop predictions of the proposed lower-fidelity models with the high-fidelity SCR model, and confirms that both models accurately approximate the high-fidelity model. In fact, it shows that *2-state lower-fidelity model*'s open-loop predictions are nearly identical to the predictions of the *5-state lower-fidelity model*. For the purpose of the comparison I simulated both models with variable-step solver `ode15s` as implemented in MATLAB.

The proposed lower-fidelity models show the the biggest inaccuracy in the interval 399–415 s, immediately after initiation of urea injection. Fig. 5.11 shows the problem in more detail. Lower-fidelity models react more quickly to inlet NH_3 step and start to reduce NO_x faster than high-fidelity model. But at the same time, they predict nearly identical NH_3 coverage ratio θ_1. As θ_1 gets higher, predictions of all models converge together. This suggests that the higher-fidelity model likely includes further θ_1-dependent feature to inhibit reactions rates at low θ_1 values. Besides, the visible discrepancy in θ_2 during the interval suggests that there is room for improvement either in the model design or parameter identification. Nevertheless, its inclusion significantly improved the model accuracy. Tab. 5.3 summarizes the root mean square and maximum errors of the lower-fidelity models with respect to the high-fidelity model. It shows error for total NH_3 coverage ratio θ_{tot}:

$$\theta_{tot} = \frac{\theta_1 M_1 + \theta_2 M_2}{M_1 + M_2} \tag{5.25}$$

Variable	**Unit**	**5-state model**		**2-state model**	
		RMS	max	RMS	max
NO	[ppm]	9.87	132.47	10.10	133.04
NO_2	[ppm]	17.38	297.62	18.05	304.89
NH_3	[ppm]	2.24	9.33	2.24	9.33
θ_{tot}	[10^{-3}]	6.37	8.43	6.37	8.43

Table 5.3: Error comparison over WLTC driving cycle. The table compares root mean square (RMS) error and maximum error of the two proposed lower-fidelity models with respect to high-fidelity model predictions.

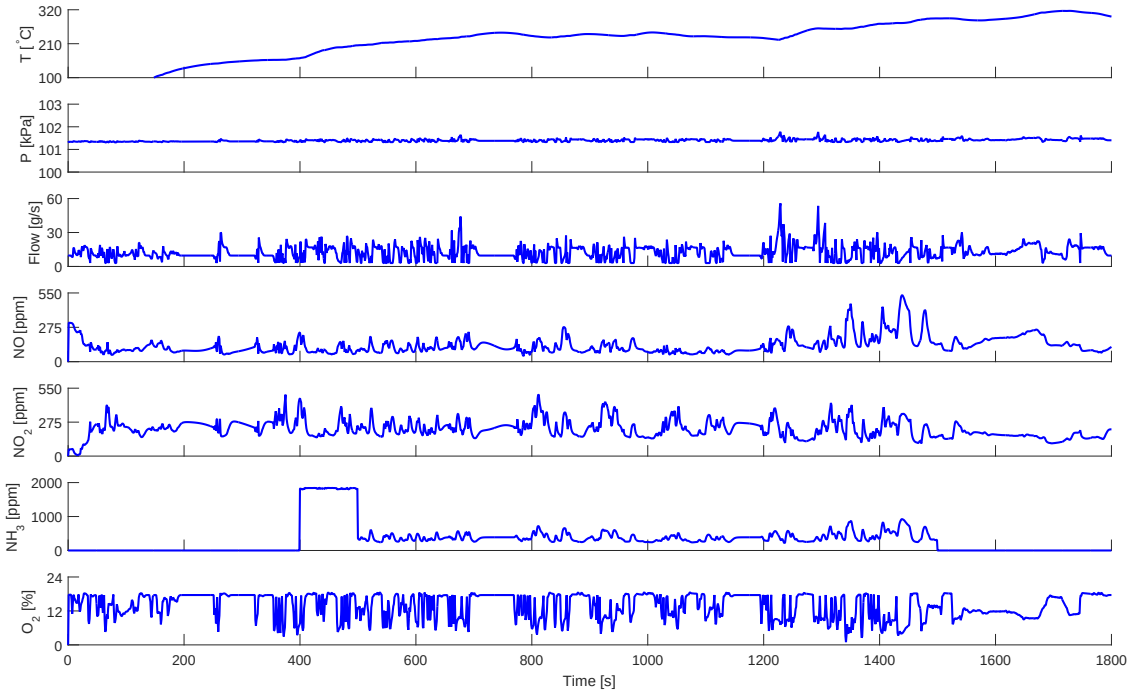

(a) inputs

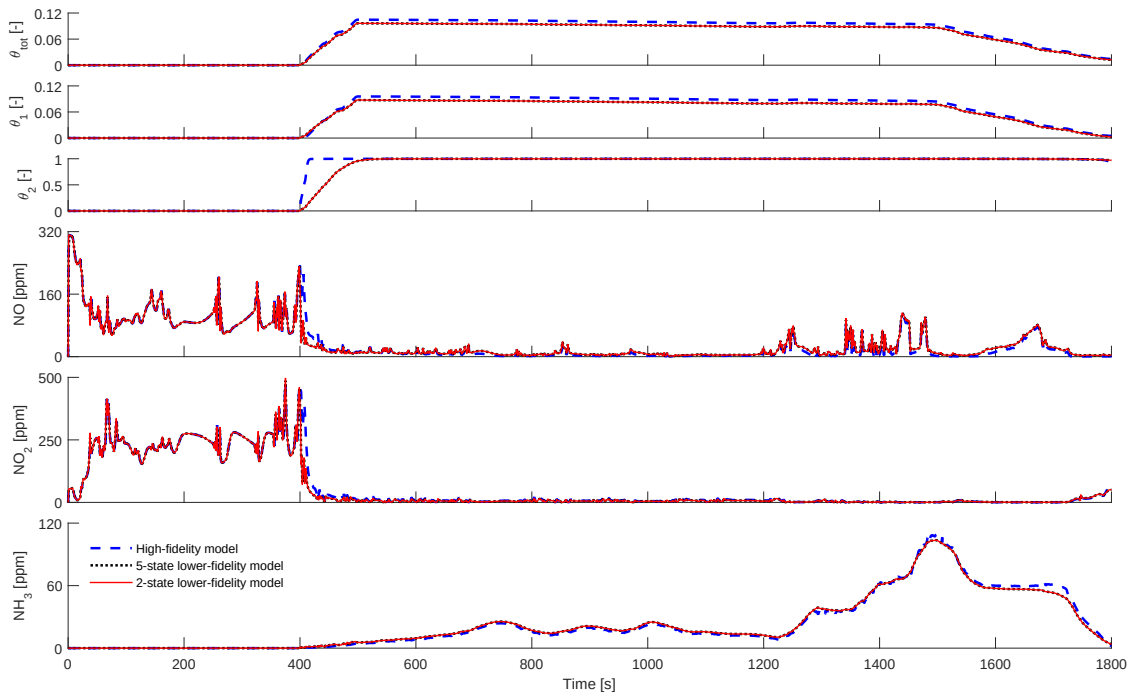

(b) outlet and internal variables

Figure 5.10: Open-loop SCR model predictions over WLTC driving cycle. Figure compares predictions of two proposed lower-fidelity models with a high-fidelity model (b) for inputs (a) over WLTC Class 3 light-duty driving cycle.

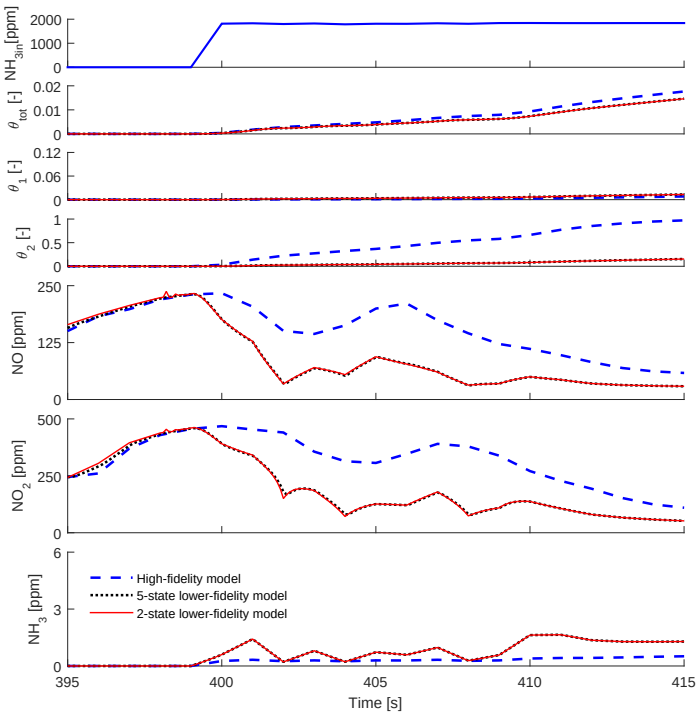

Figure 5.11: Inaccuracy after initiation of urea injection. Lower-fidelity models react more quickly to inlet NH_3 step and start to reduce NO_x faster than high-fidelity model.

Chapter 6

Development of SCR estimator

This chapter discusses development of SCR catalyst estimator for estimation of internal states and outlet specie concentrations. Section 6.1 introduces the estimation problem, specifies the measurements available, and points out simplifying assumptions. Succeeding section 6.2 introduces two Extended Kalman filter formulations: standard and numerically robust U-D algorithm. Sections 6.3 and 6.4 describe the design of estimator based on the *2-state lower-fidelity model* of SCR catalyst proposed in Chapter 5. Section 6.5 analyses estimator's performance in terms of sensitivity to perturbations of inputs and internal states, and discusses its benefits compared to open-loop model predictions.

6.1 Estimation problem

The estimation problem for the purpose of this thesis includes estimation of SCR catalyst, a part of the aftertreatment system introduced in Chapter 5. Fig. 6.1 shows the configuration schematic of the estimation problem: the estimator uses measurements of NO, NO_2 and NH_3 concentrations at the inlet of SCR, and further requires inlet pressure, inlet mass flow and internal SCR temperature. I consider three outlet measurement cases:

$$\begin{aligned} \text{(I)}&: \ NO_x \\ \text{(II)}&: \ NH_3 \\ \text{(III)}&: \ NO_x \text{ and } NH_3 \end{aligned}$$

Since NO and NO_2 can be separately measured only in laboratory conditions, these cases include all potential measurement combinations that could be used for SCR estimation onboard vehicle. The proposed estimator can provide estimates of:

- **NH_3 coverage ratio** θ_{tot} (5.25) to serve as a controlled variable for advanced control
- **outlet NH_3 concentration** to allow control with bounded NH_3 slip without utilizing NH_3 sensor
- **outlet NO and NO_2 concentrations** as input estimates for downstream catalysts

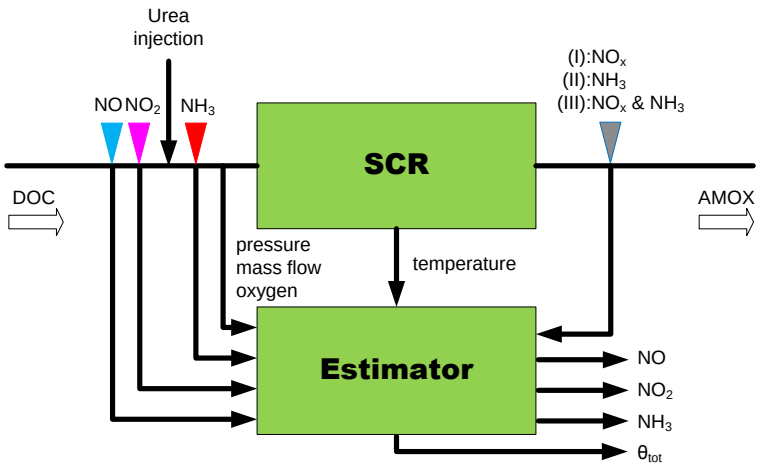

Figure 6.1: SCR estimation schematic. The estimator combines predictions of control-oriented SCR model with measurements taken at the inlet and the outlet of the SCR to estimate internal states and unmeasured outputs.

The estimation problem involves several simplifications:

- **Internal SCR temperature is available to the estimator.** In practice, internal temperature can be calculated from inlet and outlet temperature measurements. For better accuracy, a thermal model to describe heat transfer in the catalyst can be added.
- **Inlet measurements include NO and NO_2 concentrations.** Production NO_x sensors are unable to distinguish between NO and NO_2 in the exhaust gas. Either estimators of the aftertreatment systems located upstream of the SCR can provide their corresponding concentrations, or SCR estimator can include the NO_2/NOx ratio as unknown input estimate.
- **Inlet measurements include NH_3 concentration.** I consider ideal measurement of NH_3 at the inlet of the catalyst. In practice, as I discussed in Chapter 4, inlet NH_3 concentration is calculated from urea injectors and engine-out mass-flow measurements, often under the assumption of complete urea-to-NH_3 conversion, and consequently becomes a source of input uncertainty.
- **Outlet NO_x sensors provide ideal measurement.** In practice, NO_x sensors are cross-sensitive to NH_3, and this phenomenon is temperature dependent. Section 4.2 discusses the problem in more detail.

While the overall project aims at developing a robust and reliable online estimator embedded onboard vehicle to provide estimates of controlled variables, the scope of this thesis is limited to a proof-of-concept design of a control-oriented model and SCR estimator. Implementation of the designed estimator for simulation onboard vehicle, or design of a controller that utilizes estimated variables is beyond the scope of the thesis.

Literature review in Chapter 4 revealed that a multitude of various estimation design approaches were applied on the given problem in the past. I selected Extended Kalman filter to accomplish the task, an estimation approach well known in the academia, yet a novelty in the automotive industry.

6.2 Extended Kalman filter

For a linear system with white, zero-mean, and uncorrelated process and measurement noise, Kalman filter is an optimal linear filter with respect to the mean of the estimation error. Ex-

tended Kalman filter (EKF) is an extension of Kalman filter for nonlinear systems. After each measurement and time update, EKF linearizes the system around last state estimate and a Kalman filter based on the linearized model produces the next state estimate.

I introduce two formulations of Extended Kalman filter in the paragraphs below. The **standard formulation** is often not viable for hardware implementation, since it is sensitive to numerical errors [92]. While a wide range of alternative EKF formulations were proposed to address this issue, I chose to implement a **U-D filter formulation**.

The algorithms below consider a discrete-time nonlinear system:

$$x_k = f_{k-1}(x_{k-1}, u_{k-1}) + w_{k-1}, \tag{6.1}$$
$$y_k = h_k(x_k, u_k) + v_k \tag{6.2}$$

with uncorrelated white and zero-mean process and measurement noise w and v. For simplicity, I assume error covariances constant in time:

$$E(w_k w_k^{\mathrm{T}}) = Q_{\mathrm{cov}}, \tag{6.3}$$
$$E(v_k v_k^{\mathrm{T}}) = R_{\mathrm{cov}}. \tag{6.4}$$

In the text below $x_{k|k-1}$ denotes estimate of state at time k computed after measurement at time $k-1$, while $x_{k|k}$ denotes updated estimate after measurement for time k becomes available. Notation for error covariance matrix P is similar.

6.2.1 Standard formulation

Time update

Simulation of the system provides a state estimate for the following time step $x_{k|k-1}$. Error covariance propagation considers system linearized around the last estimate $x_{k-1|k-1}$. $P_{k|k-1}$ is a solution of discrete Lyapunov equation [93].

$$x_{k|k-1} = f_{k-1}(x_{k-1|k-1}, u_{k-1}) \tag{6.5}$$
$$F_{k-1} = \left.\frac{\partial f_{k-1}}{\partial x}\right|_{x_{k-1|k-1}} \tag{6.6}$$
$$P_{k|k-1} = F_{k-1} P_{k-1|k-1} F_{k-1}^{\mathrm{T}} + Q_{\mathrm{cov}} \tag{6.7}$$

Measurement update

Measurement update of both state and error covariance estimates requires computation of Kalman gain K_k from system linearized around the last estimate $x_{k|k-1}$ [93]:

$$H_k = \left.\frac{\partial h_k}{\partial x}\right|_{x_{k|k-1}} \tag{6.8}$$
$$K_k = P_{k|k-1} H_k^{\mathrm{T}} \left(H_k P_{k|k-1} H_k^{\mathrm{T}} + R_{\mathrm{cov}}\right)^{-1} \tag{6.9}$$
$$x_{k|k} = x_{k|k-1} + K_k \left(y_k - h(x_{k|k-1}, u_k)\right) \tag{6.10}$$
$$P_{k|k} = (I - K_k H_k) P_{k|k-1} \tag{6.11}$$

6.2.2 U-D filter formulation

U-D filter propagates U and D factors of error covariance P rather than the matrix itself to increase robustness of the Extended Kalman filter to numerical errors. U-D decomposition (Modified Cholesky decomposition) [92] gives the unit upper triangular U and diagonal D factors:

$$P = UDU^{\mathrm{T}}. \tag{6.12}$$

The measurement and time update algorithms of U-D filter were published by Bierman [94] and Thornton [95]. In the paragraphs below I introduce the idea of U-D error covariance propagation. I do not discuss the full algorithms for implementation in code and leave them for the interested reader to find in the above cited references. State estimate calculations follow similar idea as in the standard formulation of EKF, and thus I omitted reformulating them with U-D factors. Note that the algorithms do not require computing P from the propagated U and D factors.

Measurement update

Bierman's measurement update sequentially processes measurements one-by-one as scalars, the algorithm is executed for each measurement that becomes available at time k. The sequential approach requires diagonal measurement covariance matrix R_{cov}. A constant non-diagonal R_{cov} can be factored into diagonal R_{cov} and the measurement update algorithm is then executed with decorrelated measurements [92]. For simplicity, I consider diagonal R_{cov} in the following derivation and throughout the thesis.

After dropping time for ease of notation, denoting ith row of H as H_i, and considering P factorized as in (6.12), I can reformulate (6.9) to read:

$$K_i = P_{i-1}H_i^{\mathrm{T}}/\alpha, \tag{6.13}$$

where $\alpha = \left(H_i P_{i-1} H_i^{\mathrm{T}} + R_i\right)$. Error covariance measurement update from eq. (6.11) then becomes:

$$P_i = P_{i-1} - K_i H_i P_{i-1} \tag{6.14}$$

$$U_i D_i U_i^{\mathrm{T}} = U_{i-1} D_{i-1} U_{i-1}^{\mathrm{T}} - \frac{1}{\alpha_i} U_{i-1} D_{i-1} U_{i-1}^{\mathrm{T}} H_i^{\mathrm{T}} H_i U_{i-1} D_{i-1} U_{i-1}^{\mathrm{T}} \tag{6.15}$$

$$= U_{i-1}\left[D_{i-1} - \frac{1}{\alpha_i} D_{i-1} U_{i-1}^{\mathrm{T}} H_i^{\mathrm{T}} \left(D_{i-1} U_{i-1}^{\mathrm{T}} H_i^{\mathrm{T}}\right)^{\mathrm{T}}\right] U_{i-1}^{\mathrm{T}}. \tag{6.16}$$

Applying U-D decomposition on the term in brackets in eq. (6.16) above yields $\bar{U}\bar{D}\bar{U}^{\mathrm{T}}$ and the updated U_i and D_i factors are then:

$$U_i D_i U_i^{\mathrm{T}} = U_{i-1} \bar{U} \bar{D} \bar{U}^{\mathrm{T}} U_{i-1}^{\mathrm{T}} \tag{6.17}$$

$$= (U_{i-1}\bar{U})\bar{D}(U_{i-1}\bar{U})^{\mathrm{T}} \tag{6.18}$$

$$U_i = U_{i-1}\bar{U} \tag{6.19}$$

$$D_i = \bar{D}. \tag{6.20}$$

Time update

I assume diagonal process covariance matrix Q_{cov} to simplify the following derivation, the idea remains identical for non-diagonal Q_{cov}. The error covariance update from eq. (6.7) with F_{k-1}

as in (6.6) can be reformulated with U-D factorized P as follows:

$$P_{k|k-1} = F_{k-1}P_{k-1|k-1}F_{k-1}^{\mathrm{T}} + Q_{\mathrm{cov}} \tag{6.21}$$

$$= \begin{bmatrix} F_{k-1}U_{k-1|k-1} & I \end{bmatrix} \begin{bmatrix} D_{k-1|k-1} & 0 \\ 0 & Q_{\mathrm{cov}} \end{bmatrix} \begin{bmatrix} U_{k-1|k-1}^{\mathrm{T}} F_{k-1}^{\mathrm{T}} \\ I \end{bmatrix} \tag{6.22}$$

$$= W\tilde{D}W^{\mathrm{T}} \tag{6.23}$$

$$U_{k|k-1}D_{k|k-1}U_{k|k-1}^{\mathrm{T}} = W\tilde{D}W^{\mathrm{T}} \tag{6.24}$$

To find the updated $U_{k|k-1}$ and $D_{k|k-1}$ factors Thornton's algorithm uses Modified Weighted Gram-Schmidt orthogonalization on the right-hand side of eq. (6.24) to produce

$$W = U_{k|k-1}V, \tag{6.25}$$

and consequently

$$D_{k|k-1} = V\tilde{D}V^{\mathrm{T}}. \tag{6.26}$$

6.3 EKF for nonlinear DAE system

A nonlinear continuous-time DAE model with states x, algebraic variables a and inputs u can be formulated in the following semi-explicit form:

$$\begin{aligned} \dot{x} &= f(x,a,u) \\ 0 &= g(x,a,u) \\ y &= h(x,a,u). \end{aligned} \tag{6.27}$$

To apply discrete-time Extended Kalman filter on such a model, it has to be linearized and discretized. To linearize the model I followed a procedure well described in [96]. I let $\varphi(\dot{x},x,a,u) = \dot{x} - f(x,a,u) = 0$ and denote partial derivatives by subscripts to get:

$$\Delta\dot{x} = A\Delta x + B\Delta u = \left[\varphi_a g_a^{-1} g_x - \varphi_x\right]\Delta x + \left[\varphi_a g_a^{-1} g_u - \varphi_u\right]\Delta u \tag{6.28}$$

$$\Delta y = C\Delta x + D\Delta u = \left[h_x - h_a g_a^{-1} g_x\right]\Delta x + \left[h_u - h_a g_a^{-1} g_u\right]\Delta u \tag{6.29}$$

Explicit Forward Euler discretization gives:

$$\begin{aligned} x_k &= x_{k-1} + f(x_{k-1}, a_{k-1}, u_{k-1})\Delta t \\ 0 &= g(x_k, a_k, u_k) \\ y_k &= h(x_k, a_k, u_k) \end{aligned} \tag{6.30}$$

The Jacobian matrices of the system and output function, as defined in (6.6) and (6.8), are then:

$$\begin{aligned} F_{k-1} &= \left.\frac{\partial f_{k-1}}{\partial x}\right|_{x_{k-1|k-1}} &&= I + A|_{x_{k-1|k-1}}\Delta t \\ H_k &= \left.\frac{\partial h_k}{\partial x}\right|_{x_{k|k-1}} &&= C|_{x_{k|k-1}} \end{aligned} \tag{6.31}$$

6.4 EKF for SCR catalyst

The nonlinear *2-state lower-fidelity model* of SCR catalyst—formulated in Chapter 5—fits the semi-explicit DAE form in eq. (6.27). To implement the discrete-time U-D Extended Kalman filter, I discretized the model as described in previous section. The nonlinear discrete-time model for EKF comprises:

- states – NH_3 coverage ratios of 1st and 2nd site: θ_1, θ_2
- algebraic variables – concentrations of NO, NO_2, NH_3: C_{NO}, C_{NO_2}, C_{NH_3}
- inputs – inlet concentrations of NO, NO_2, NH_3, O_2, temperature, exhaust gas, mass flow and inlet pressure: $C_{NO_{in}}$, $C_{NO_{2in}}$, $C_{NH_{3in}}$, $C_{O_{2in}}$, T, $\dot{m}$, P_{in}

For ease of notation I denote the next time step by $^+$ and omit other time indices, the model then reads:

$$\begin{bmatrix}\theta_1\\ \theta_2\end{bmatrix}^+ = \begin{bmatrix}\theta_1\\ \theta_2\end{bmatrix} + \begin{bmatrix}\frac{1}{M_1}\left(r_{ads_1} - r_{des_1} - 2r_{std} - 8r_{slow} - 2r_{fast} - 4r_{oxi}\right)\\ \frac{1}{M_2}\left(r_{ads_2} - r_{des_2}\right)\end{bmatrix}\Delta t \tag{6.32}$$

$$\begin{bmatrix}0\\0\\0\end{bmatrix} = \begin{bmatrix}-\frac{\nu}{L}\left(C_{NO} - C_{NO_{in}}\right) - 2r_{std} - r_{fast}\\ -\frac{\nu}{L}\left(C_{NO_2} - C_{NO_{2in}}\right) - 6r_{slow} - r_{fast}\\ -\frac{\nu}{L}\left(C_{NH_3} - C_{NH_{3in}}\right) - r_{ads_1} + r_{des_1} - r_{ads_2} + r_{des_2}\end{bmatrix} \tag{6.33}$$

$$\begin{aligned} r_{ads_1} &= k_{ads_1} C_{NH_3}(1-\theta_1) M_1, & r_{ads_2} &= k_{ads_2} C_{NH_3}(1-\theta_2) M_2,\\ r_{des_1} &= k_{des_1}\theta_1 M_1, & r_{des_2} &= k_{des_2}\theta_2 M_2,\\ r_{std} &= k_{std} C_{NO}\theta_1 M_1, & r_{fast} &= k_{fast} C_{NO} C_{NO_2}\theta_1 M_1,\\ r_{slow} &= k_{slow} C_{NO_2}\theta_1 M_1, & r_{oxi} &= k_{oxi} C_{O_{2in}}\theta_1 M_1 \end{aligned} \tag{6.34}$$

where $k_i = A_i e^{\frac{E_i}{RT}}$ for $i = ads_1, ads_2, des_1, des_2$, std, fast, slow, oxi. I assume all concentrations in mol/m^3. Ideal gas law is used for unit conversion of inlet specie concentrations from ppm to mol/m^3 as in eq. (5.10). Gas flow velocity ν is computed from mass flow $\dot{m}$ and inlet pressure P_{in} as discussed in section 5.4:

$$\nu = \frac{\dot{m} M_{gas}}{A_f P_{in} R T}. \tag{6.35}$$

NH_3 concentration C_{NH_3} can be expressed explicitly from eq. (6.33). Quadratic equation has to be solved to get solution to C_{NO} and C_{NO_2}. For physically feasible values, the solution can always be found. I used symbolic math solver to get analytical solution to the quadratic equation and to obtain Jacobian matrices given in (6.31) from the linearized model in (6.28) and (6.29). The resulting bulky expressions provide little additional information for the reader and thus I decided to omit them from the text. I consider discussion on model observability or criteria of stability beyond the scope of this thesis, simulations in section 6.5 confirm that the model is feasible for implementation in the EKF.

The following algorithm summarizes the implemented U-D Extended Kalman filter for SCR catalyst:

1. Specify initial P_0 and x_0
2. Apply U-D decomposition on P_0 (6.12)
3. At each time k:
   (a) Calculate concentrations $a_{k|k-1}$ from algebraic equations (6.33).

(b) *Measurement update:*
   i. Let $x^0 = x_{k|k-1}$, $a^0 = a_{k|k-1}$, $U^0 = U_{k|k-1}$, and $D^0 = D_{k|k-1}$.
   ii. For each scalar in the vector of measurements $i = 1, 2, \ldots, m$:
      A. Run Bierman's algorithm to get x^i, U^i and D^i.
      B. Calculate concentrations a^i from algebraic equations (6.33).
   iii. Let $x_{k|k} = x^m$, $a_{k|k} = a^m$, $U_{k|k} = U^m$, and $D_{k|k} = D^m$.
(c) *Time update:* Run Thornton's algorithm to get $x_{k+1|k}$, $U_{k+1|k}$, $D_{k+1|k}$.

Process noise covariance matrix Q_{cov} and measurement noise covariance matrix R_{cov} serve as tuning parameters. I assume independent noise vector components by considering both matrices diagonal. I let the sampling time $\Delta t = 0.1\,s$ in all simulations.

6.5 Simulations and discussion

6.5.1 Validation and robustness analysis

I performed series of simulations to validate the proposed Extended Kalman filter and to analyze its robustness to perturbations in inputs and internal states. Fig. 6.2 shows a configuration schematic for the validation experiments. Outputs of perturbed *2-state lower-fidelity model* serve as measurements for the designed estimator. The Extended Kalman Filter internally uses identical model, but it receives unperturbed inputs.

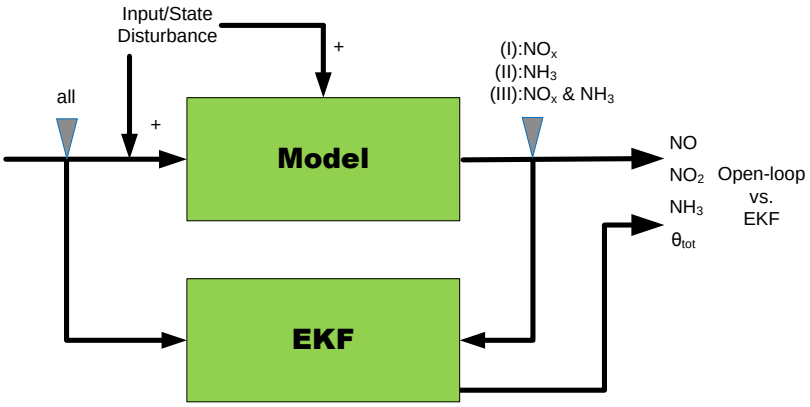

Figure 6.2: EKF validation and robustness analysis. Open-loop model is perturbed in inlet concentrations and internal states, EKF with identical model uses the predictions of open-loop model as measurements. This serves to validate EKF functionality and to analyze its robustness.

I performed experiments for perturbations in internal state θ_1, inlet NO_x, NO_2, NH_3, oxygen, exhaust mass flow, and temperature. Fig. 6.3—6.9 compare estimated internal states and outlet NO, NO_2, NH_3 concentrations with the perturbed open-loop predictions for all three outlet measurement cases: NO_x, NH_3, and both NO_x and NH_3. To simplify showcasing the results, the figures show total NH_3 coverage ratio θ_{tot} rather than separate θ_1 and θ_2 as defined in 5.25.

In the following experiments, I tuned R_{cov} to react quickly to measurements, while keeping Q_{cov} the same for all experiments.

Perturbation of θ_1, inlet NH_3 and inlet oxygen The Extended Kalman filter is by design robust to noise, and—subject to tuning of Q_{cov} and R_{cov} matrices—also to perturbations in its internal states θ_1 and θ_2. Fig. 6.3 shows that this is indeed the case for any outlet measurements available as it correctly estimates all variables. Moreover, proposed EKF achieves similar results for perturbation of inlet NH_3 and inlet oxygen, which affect the NH_3 storage directly through NH_3 adsorption reactions and NH_3 oxidation reaction, respectively. Therefore, it can easily correct the perturbation by manipulating NH_3 coverage ratios θ_1 and θ_2.

Perturbation of exhaust mass flow As Fig. 6.6 shows, when exhaust mass flow is perturbed the estimator is unable to provide accurate estimates for all variables at the same time. With NO_x measurements, it correctly estimates outlet NO and NO_2 concentrations, but only at the cost of inaccuracy in outlet NH_3 and θ_{tot}. Estimation with NH_3 measurements yields opposite results. Using both NO_x and NH_3 measurements does not improve estimation.

The structure of the underlying model does not allow the estimator to manipulate θ_{tot} and internal concentrations independently, as they are coupled by the algebraic equations (6.33). The perturbation of mass flow affects flow velocity (6.35), which features in the algebraic equations, and consequently introduces error in the coupling between the internal states and algebraic variables.

In the end, the experiment shows that the underlying model is robust to mass flow error, 20% perturbation has negligible effect on θ_{tot} and $\sim 5\%$ on outlet NO and NO_2 concentrations. Note that perturbation of inlet pressure would yield similar results, as it affects the flow velocity similarly to mass flow.

Perturbation of temperature Experiment results in Fig. 6.7 show that the open-loop model is sensitive to temperature. The EKF does not provide accurate θ_{tot}, NO, NO_2 or NH_3 estimates with any outlet measurements. The structure of the underlying model does not allow the EKF to accurately respond to perturbations by manipulating its internal states. The reasons are similar as for the exhaust mass flow perturbation: temperature change affects temperature-dependent reaction rates with different magnitudes and introduces error in coupling between the internal and algebraic states represented by algebraic equations (6.33). This problem can be solved by including temperature model and the temperature as a state into the EKF as in [58].

Perturbation of inlet NO_x Fig. 6.8 shows that using NH_3 outlet measurements gives better results as the EKF estimates θ_{tot} accurately and captures the trend in NO and NO_2 concentrations. With NO_x measurements the estimator provides slightly better NO and NO_2 estimates, but fails to provide accurate NH_3 and θ_{tot}. Overall, both the underlying model and the estimator show sensitivity to perturbation of inlet NO_x concentrations.

Perturbation of inlet NO_2 This experiment analyses sensitivity of the estimator to perturbation in inlet NO_2/NO_x ratio. NH_3 outlet measurements allow the EKF to accurately estimate θ_{tot}, but add little benefit for estimation of outlet NO and NO_2 concentrations. Outlet NO_x measurements make the EKF respond to the perturbation by manipulating θ_{tot} overly aggressively. It provides estimates less accurate than open-loop model predictions. This is the only experiment where EKF shows disadvantage over open-loop model.

The following points summarize the main takeaways from above discussed experiments:

- EKF correctly captures perturbation of θ_1, inlet NH_3 and oxygen with either NO_x or NH_3 outlet measurements in all estimated variables
- EKF is sensitive to perturbation of temperature, exhaust mass flow, inlet NO_x and inlet NO_2/NO_x ratio
- When temperature is perturbed, EKF is unable to accurately estimate NO, NO_2, NH_3 nor θ_{tot} with any outlet measurements.
- EKF shows benefit over open-loop model in all but one experiment: perturbation of NO_2/NO_x ratio with outlet NO_x measurements available.
- Estimates cannot be improved in any of the experiments by using both NO_x and NH_3 outlet measurements

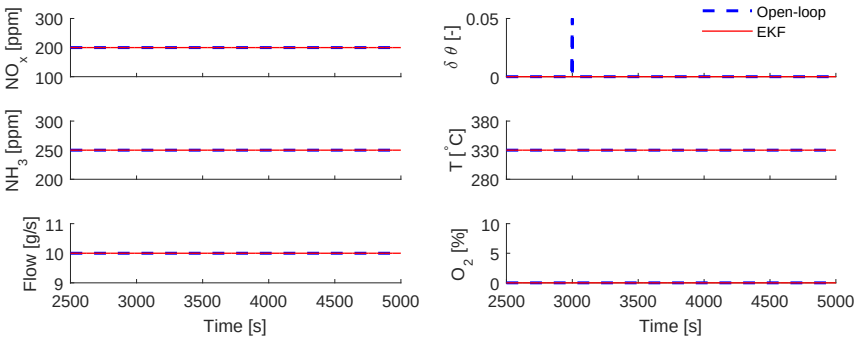

(a) inputs and perturbation of θ_1

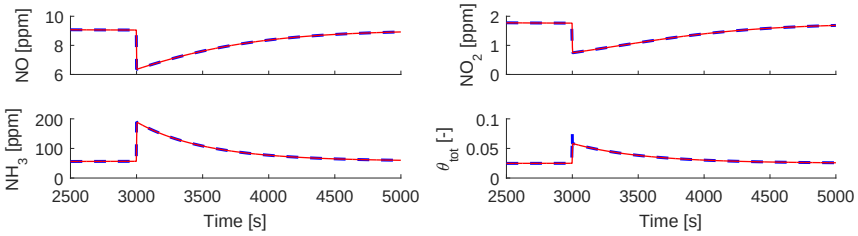

(b) outlet NO_x measurements

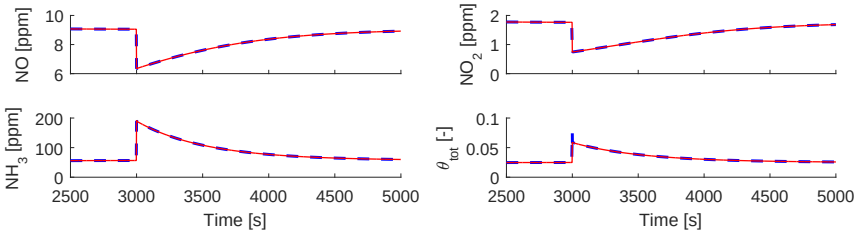

(c) outlet NH_3 measurements

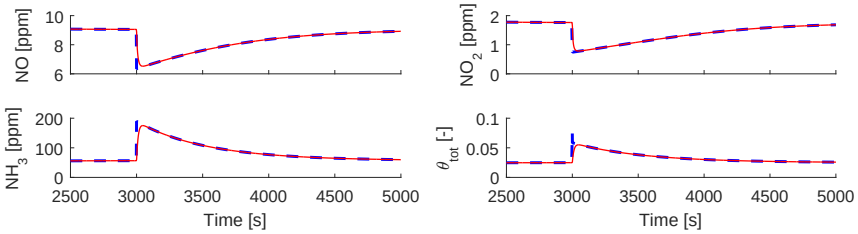

(d) outlet NO_x and NH_3 measurements

Figure 6.3: Perturbation of θ_1. When internal states are perturbed, either NO_x or NH_3 measurements provide sufficient information for the EKF to provide accurate estimates of all variables.

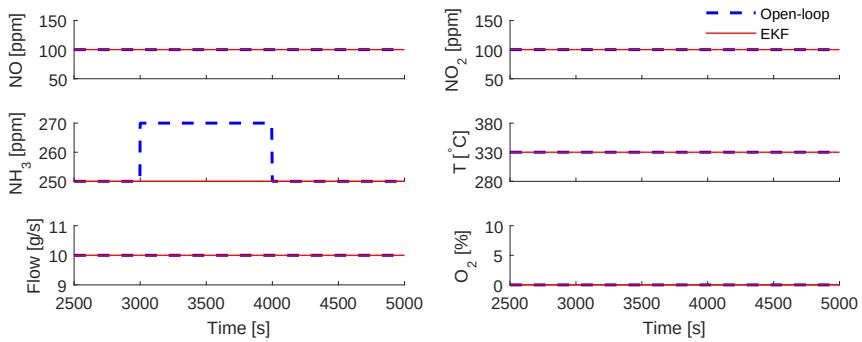

(a) inputs

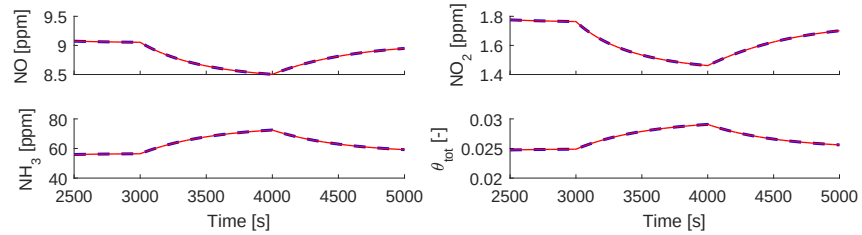

(b) outlet NO_x measurements

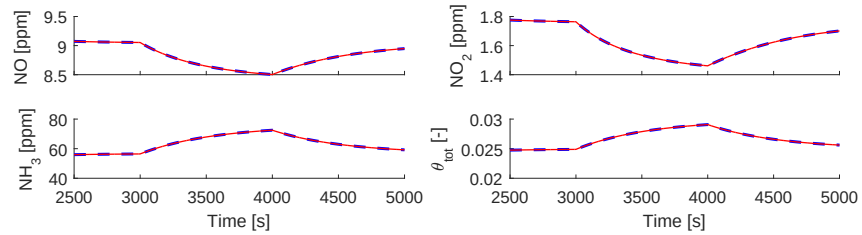

(c) outlet NH_3 measurements

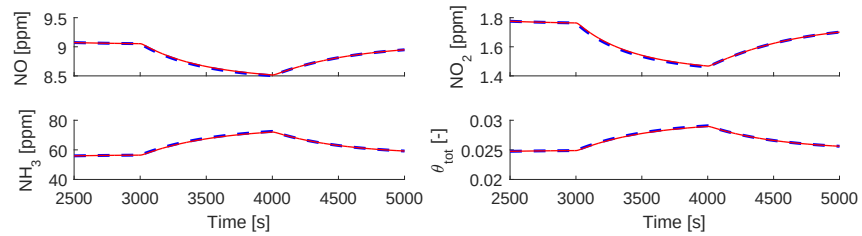

(d) outlet NO_x and NH_3 measurements

Figure 6.4: Perturbation of inlet NH_3 concentration. When inlet NH_3 is perturbed, either NO_x or NH_3 measurements provide sufficient information for the EKF to provide accurate estimates of all variables.

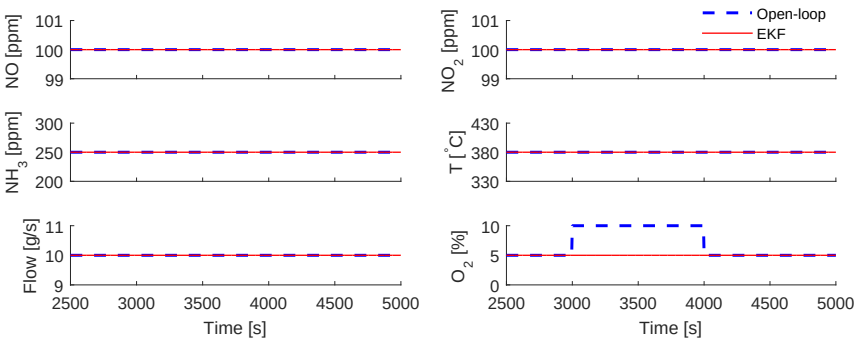

(a) inputs

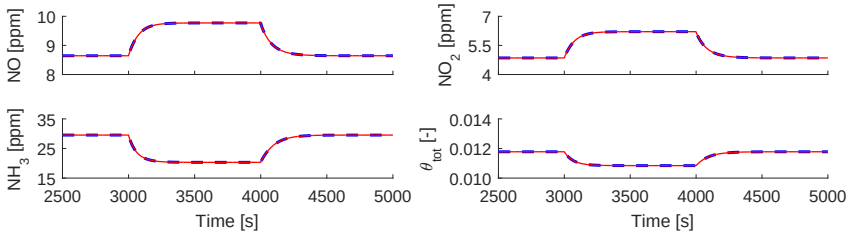

(b) outlet NO_x measurements

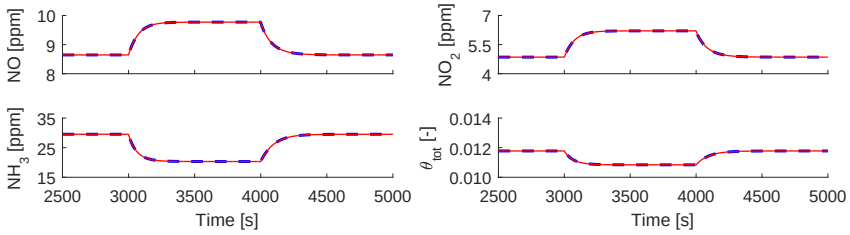

(c) outlet NH_3 measurements

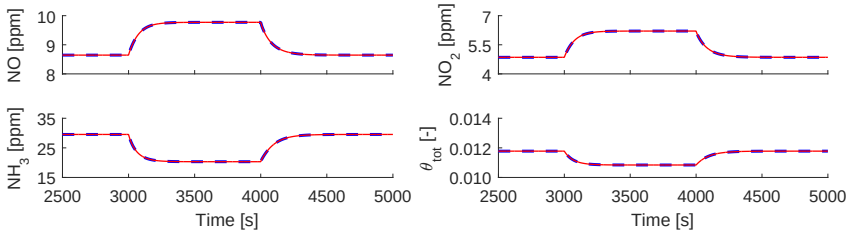

(d) outlet NO_x and NH_3 measurements

Figure 6.5: Perturbation of inlet O_2 concentration. When inlet NH_3 is perturbed, either NO_x or NH_3 measurements provide sufficient information for the EKF to provide accurate estimates of all variables.

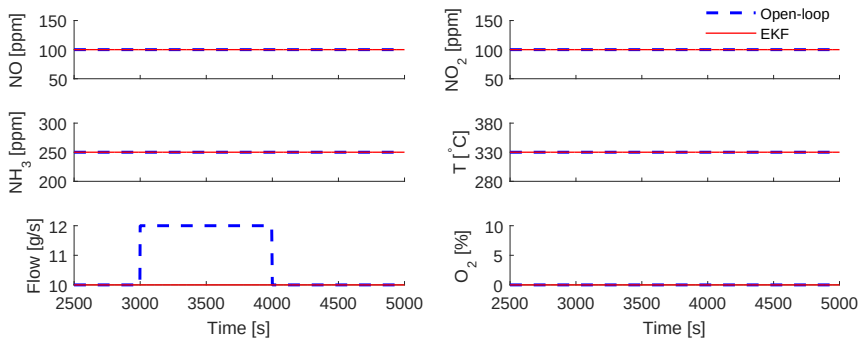

(a) inputs

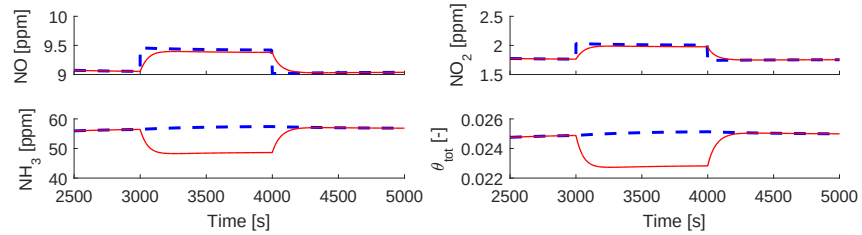

(b) outlet NO_x measurements

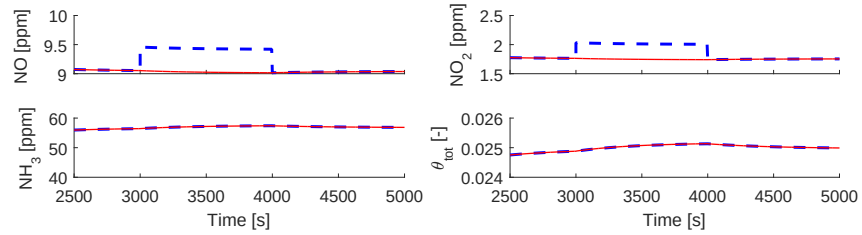

(c) outlet NH_3 measurements

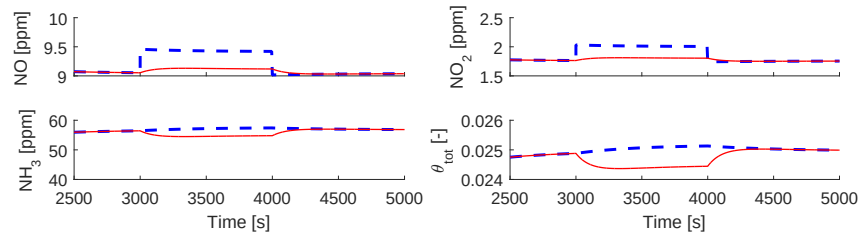

(d) outlet NO_x and NH_3 measurements

Figure 6.6: Perturbation of exhaust mass flow. Either NO and NO_2 concentrations or θ_{tot} can be estimated accurately as a trade-off between between the effect of outlet NO_x measurements and NH_3 measurements.

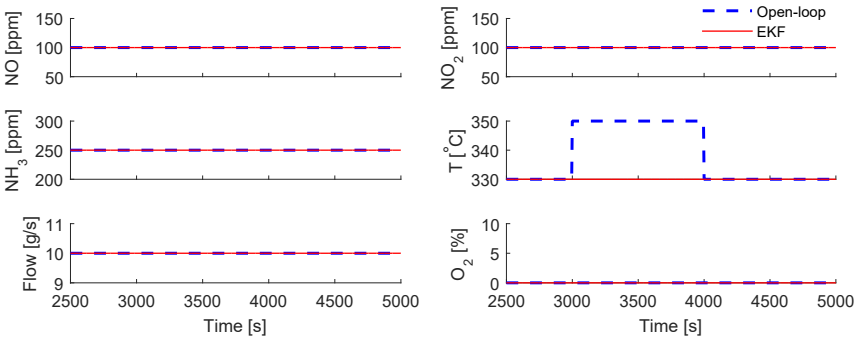

(a) inputs

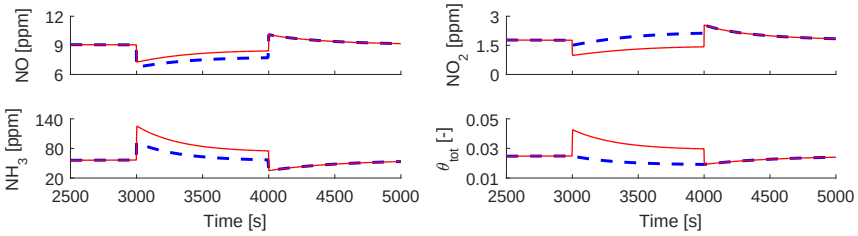

(b) outlet NO_x measurements

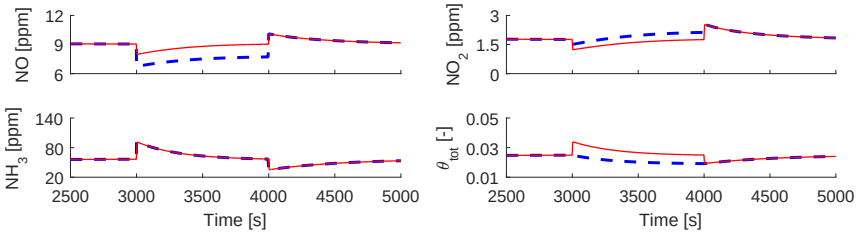

(c) outlet NH_3 measurements

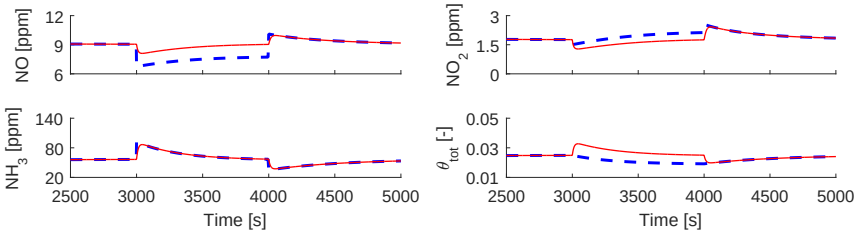

(d) outlet NO_x and NH_3 measurements

Figure 6.7: Perturbation of internal temperature. The proposed EKF is sensitive to temperature, it does not provide accurate θ_{tot}, NO, NO_2 or NH_3 estimates with any outlet measurements.

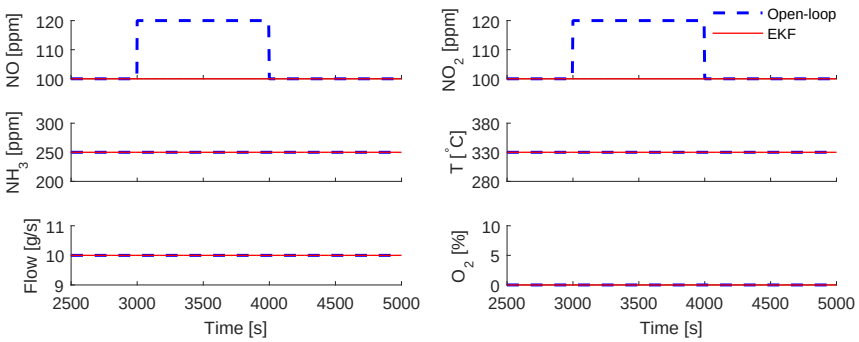

(a) inputs

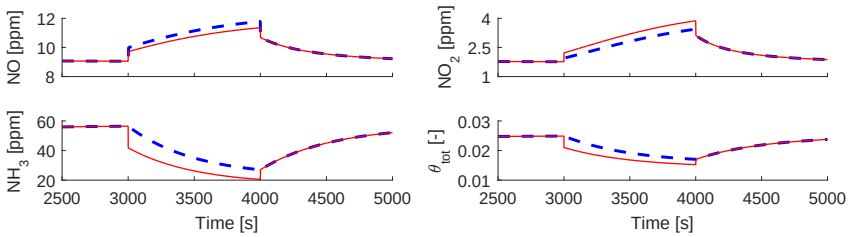

(b) outlet NO_x measurements

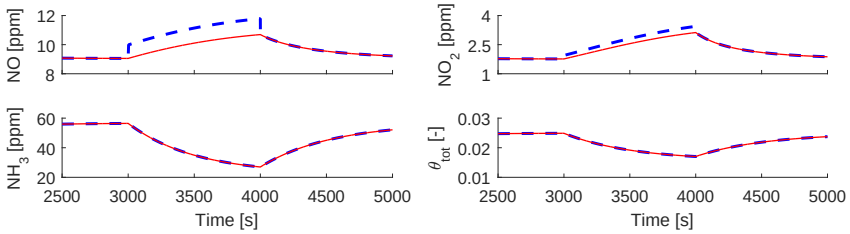

(c) outlet NH_3 measurements

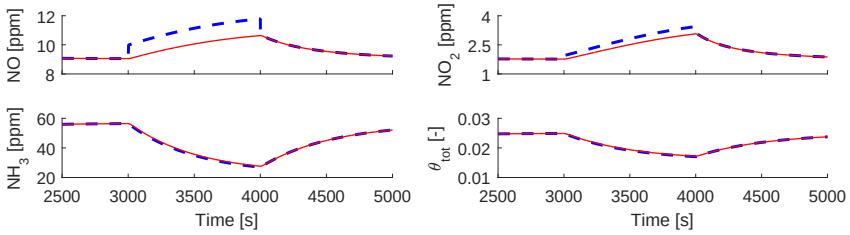

(d) outlet NO_x and NH_3 measurements

Figure 6.8: Perturbation of inlet NO_x concentration. EKF with NH_3 outlet measurements estimates θ_{tot} accurately and captures the trend in NO and NO_2 concentrations. With NO_x measurements, the estimator provides slightly better NO and NO_2 estimates, but fails to provide accurate NH_3 and θ_{tot}.

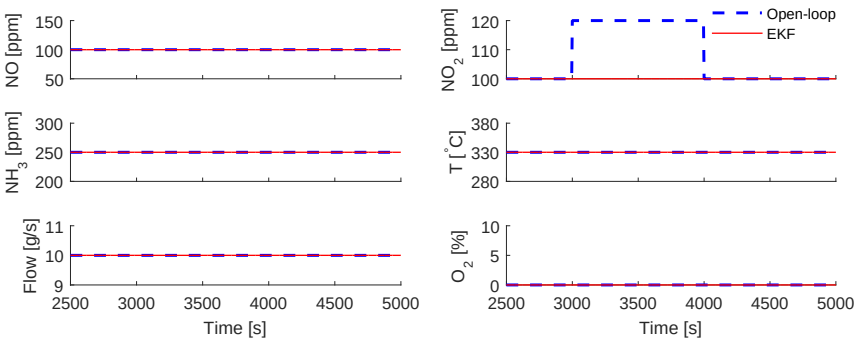

(a) inputs

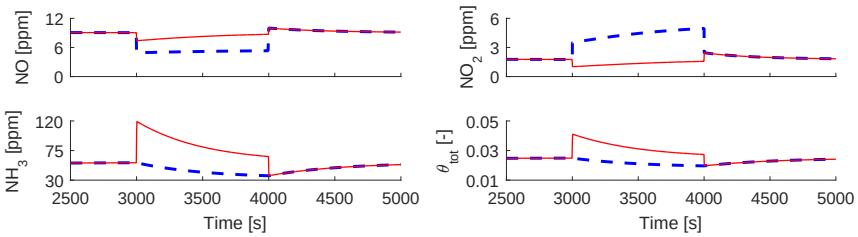

(b) outlet NO_x measurements

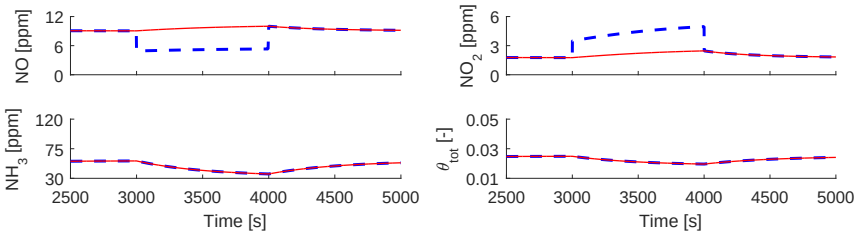

(c) outlet NH_3 measurements

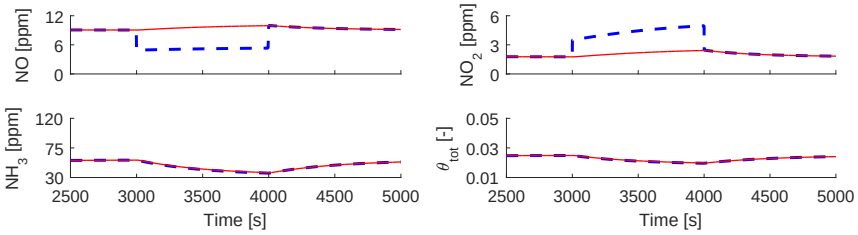

(d) outlet NO_x and NH_3 measurements

Figure 6.9: Perturbation of inlet NO_2 concentration. The proposed EKF is very sensitive to perturbation of NO_2/NO_x ratio. With NO_x outlet measurements the EKF estimates are worse than open-loop predictions. With NH_3 measurements it does not capture peaks in NO and NO_2 concentrations.

6.5.2 Estimation over a driving cycle

I analyzed prediction accuracy of the proposed lower-fidelity models in open-loop simulation over a WLTC Class 3 light-duty driving cycle [91] in Chapter 5. The following discussion concerns application of the proposed Extended Kalman Filter on the similar data. Simulations of a diesel engine model—calibrated in Honeywell's ONRAMP DESIGN SUITE—provided engine-out data for a high-fidelity aftertreatment model, which in turn provided inputs for the proposed *2-state lower-fidelity model* of SCR catalyst and output measurements for the estimator.

Fig. 6.10 compares estimates of a fine-tuned EKF, which uses outlet NO_x measurements, with open-loop predictions of the high-fidelity and *2-state lower-fidelity* models. Since open-loop simulations of the *2-state lower-fidelity model* show a good fit to the high-fidelity model predictions, the EKF has limited room to improve them any further.

The open-loop model predictions suffer from the biggest inaccuracy after initiation of urea injection at 399 s, the lower-fidelity model predicts much less NO_x than the higher-fidelity model. Fig. 6.11 shows in more detail the considerable improvement in outlet NO and NO_2 concentrations introduced by the EKF, which measures the difference between outlet NO_x predictions and measurements and responds by manipulating θ_1 to slow down the NO_x reducing reactions.

I repeated the simulations for all three outlet measurement combinations and summarized the results in Tab. 6.1. EKF with NH_3 outlet measurements has negligible effect on accuracy of estimates since NH_3 measurements do not provide any information about the inaccuracy in NO_x predictions after the initiation of urea injection. It can be tuned—by manipulating measurement error covariance R_{cov}—to slightly decrease estimation error in outlet NH_3 concentration, but it is always at the cost of increasing error in the estimates of internal states. Consequently, EKF with both NO_x and NH_3 shows results similar to EKF with NO_x only measurements as the NH_3 measurements do not introduce much benefit to estimation accuracy.

Variable	Unit	Open-loop		NO_x		NO_x+NH_3		NH_3	
		RMS	max	RMS	max	RMS	max	RMS	max
NO	[ppm]	10.10	133.04	6.72	48.24	6.72	48.22	10.08	132.97
NO_2	[ppm]	18.05	304.89	6.75	69.64	6.54	69.55	17.94	304.68
NH_3	[ppm]	2.24	9.33	1.78	8.42	0.60	5.20	0.61	5.20
θ_{tot}	[10^{-3}]	6.37	8.43	13.27	20.73	13.10	31.61	12.51	28.24

Table 6.1: Summary of estimation error over a WLTC driving cycle. The table compares root mean square (RMS) and maximum error of open-loop model and Extended Kalman filter with respect to high-fidelity model predictions. Columns labeled NO_x, NO_x+NH_3 and NH_3 denote EKF with respective outlet measurements.

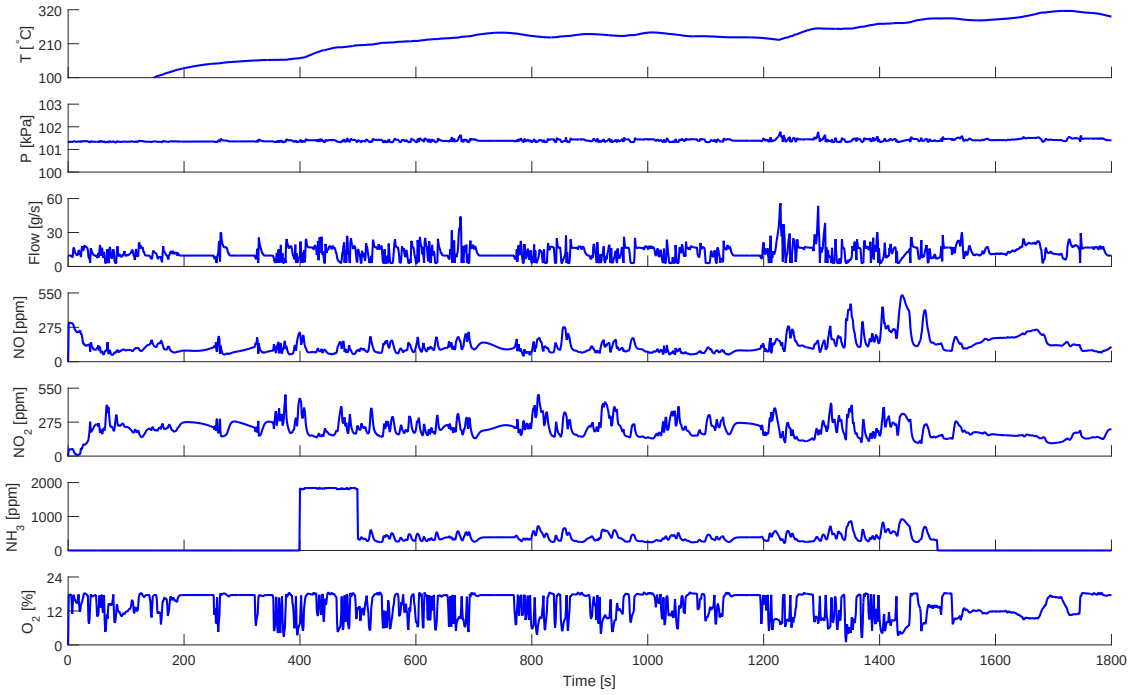

(a) inputs

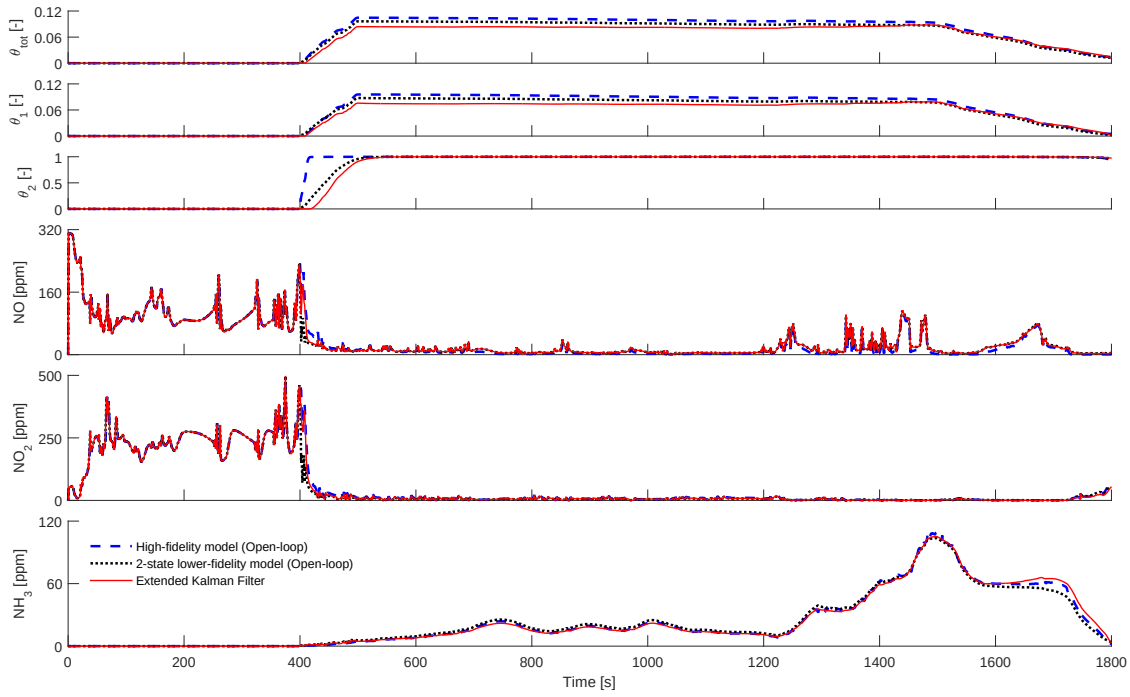

(b) outlet and internal variables

Figure 6.10: Comparison of EKF estimates with open-loop model predictions over WLTC driving cycle. Figure compares estimates of a fine-tuned EKF, which uses both outlet NO_x and NH_3 measurements, with open-loop predictions of the *2-state lower-fidelity* and high-fidelity models over WLTC Class 3 light-duty driving cycle.

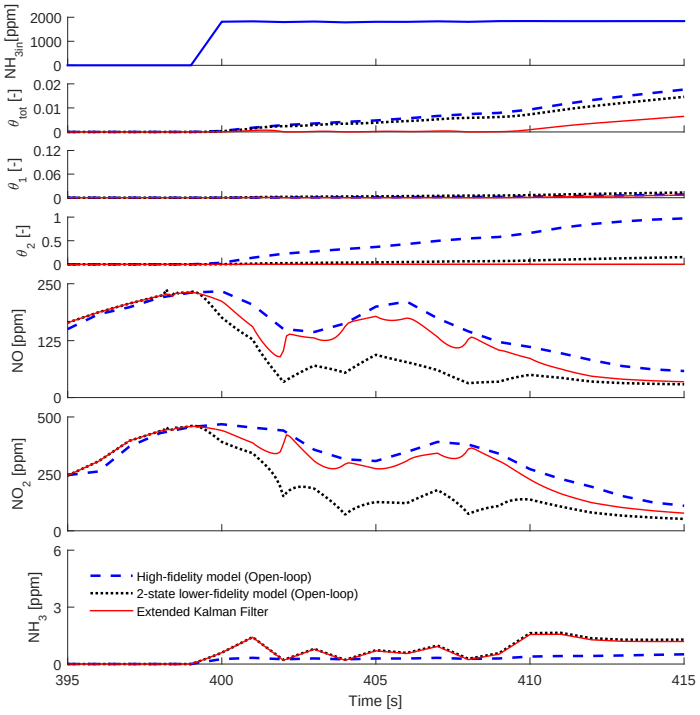

Figure 6.11: Inaccuracy after initiation of urea injection. Extended Kalman filter provides more accurate NO and NO_2 concentrations than the open-loop *2-state lower-fidelity model* by manipulating θ_1 to slow down NO_x reducing reactions.

Chapter 7

Conclusion

I proposed two nonlinear physics-based control-oriented models of SCR catalyst for implementation in an online estimator. I calibrated the models based on simulation data provided by high-fidelity aftertreatment model in a 6-step identification procedure. The *5-state lower-fidelity model*—when simulated with explicit Forward Euler numerical integration method—requires small sampling time to provide stable and accurate predictions, which makes it slow for online applications. I obtained the *2-state lower-fidelity model* by omitting dynamics of internal gas concentrations in the *5-state lower-fidelity model* to reduce the model's stiffness and consequently allow fast simulation. The simulation results over WLTC driving cycle in Chapter 5 show that both models provide nearly identical predictions, and accurately approximate predictions of the high-fidelity model.

I designed an Extended Kalman Filter for estimation of NH_3 storage and outlet NO, NO_2 and NH_3 concentrations. I implemented a U-D algorithm, which propagates factors of error covariance matrix rather than the matrix itself to increase robustness to numerical errors. The *2-state lower-fidelity model* simulated with explicit Forward Euler method provides time predictions. The EKF uses measurements of either NO_x, NH_3 or both NO_x and NH_3 outlet concentrations for the measurement update.

I performed series of simulations to validate the Extended Kalman Filter and to analyze its robustness to perturbations of inputs and internal states. The EKF is robust to perturbation of internal states and inlet concentrations of NH_3 and oxygen in any of the three outlet measurement configurations, but shows sensitivity to perturbation in exhaust mass flow, NO_x, NO_2/NO_x ratio and temperature due to limited fidelity of the proposed model: The EKF can manipulate only its internal states, the coverage ratios of two NH_3 storage sites, but the gas concentration estimates remain coupled with the internal states through algebraic equations and cannot be changed independently. Consequently, the model structure is too rigid to allow more robust estimation.

Results of simulations over WLTC driving cycle, where all the models received unperturbed noise-free inputs, show that EKF introduces only minor improvement over open-loop model predictions. Nevertheless, the EKF—despite its sensitivity to inputs—provides significant benefit over open-loop predictions for perturbed or noisy inputs.

Design of production-ready estimator is a topic for future work: It needs a degree of freedom in temperature to increase temperature robustness, it has to consider cross-sensitivity of production NO_x sensors to NH_3, and perhaps include inlet NO_2/NO_x ratio as unknown input estimate as it cannot be measured. In the end, structure of the *2-state lower-fidelity model* might be too limiting for the EKF and some of the omitted internal gas concentration dynamics would have to be reincluded. Consequently, different numerical integration method would have to be implemented to allow fast simulation with reasonable sampling time.

Bibliography

[1] "Regulation (EC) No 595/2009 of the European Parliament and of the council," Jun. 2009. [Online]. Available: http://eur-lex.europa.eu/LexUriServ/LexUriServ.do?uri=OJ:L:2009:188:0001:0013:EN:PDF

[2] "Regulation (EC) No 443/2009 of the European Parliament and of the Council," Apr. 2009. [Online]. Available: http://eur-lex.europa.eu/legal-content/EN/TXT/PDF/?uri=CELEX:02009R0443-20130508&from=EN

[3] V. Franco, F. P. Sánchez, J. German, and P. Mock, "Real-world exhaust emissions from modern diesel cars," The internation council on clean transportation, Tech. Rep., 2014. [Online]. Available: http://theicct.org/sites/default/files/publications/ICCT_PEMS-study_diesel-cars_20141010.pdf

[4] T. Johnson, "Vehicular Emissions in Review," *SAE Int. J. Engines*, no. 7(3), 2014.

[5] "EU: Heavy-duty: Emissions," 2014. [Online]. Available: http://transportpolicy.net/index.php?title=EU:_Heavy-duty:_Emissions

[6] "Heavy-Duty Onroad Engines." [Online]. Available: https://www.dieselnet.com/standards/us/hd.php

[7] "Heavy-Duty Truck and Bus Engines." [Online]. Available: https://www.dieselnet.com/standards/eu/hd.php

[8] "US: Light-duty: Emissions." [Online]. Available: http://transportpolicy.net/index.php?title=US:_Light-duty:_Emissions

[9] "EU CO2 standards for passenger cars and light-commercial vehicles." [Online]. Available: http://www.theicct.org/eu-co2-standards-passenger-cars-and-lcvs

[10] "Emission Standards - European Union Cars and Light Trucks." [Online]. Available: https://www.dieselnet.com/standards/eu/ld.php

[11] G. Zamboni and M. Capobianco, "Influence of high and low pressure EGR and VGT control on in-cylinder pressure diagrams and rate of heat release in an automotive turbocharged diesel engine," *Applied Thermal Engineering*, vol. 51, no. 1-2, pp. 586–596, Mar. 2013.

[12] G. H. Abd-Alla, "Using exhaust gas recirculation in internal combustion engines: a review," *Energy Conversion and Management*, vol. 43, no. 8, pp. 1027–1042, 2002.

[13] M. K. Khair and H. Jääskeläinen, "Exhaust Gas Recirculation." [Online]. Available: https://www.dieselnet.com/tech/engine_egr.php

[14] "Cummins unveils new QSM12 without EGR at BAUMA," Apr. 2013. [Online]. Available: https://www.dieselnet.com/news/2013/04cummins.php

[15] O. Salvat, P. Marez, and G. Belot, "Passenger Car Serial Application of a Particulate Filter System on a Common Rail Direct Injection Diesel Engine," SAE International, Warrendale, PA, SAE Technical Paper 2000-01-0473, Mar. 2000.

[16] J. Adler, "Ceramic diesel particulate filters," *International Journal of Applied Ceramic Technology*, vol. 2, no. 6, pp. 429–439, 2005.

[17] "Diesel Particulate Filters," Sep. 2007. [Online]. Available: http://www.forddoctorsdts.com/articles.html/_/dtsarticles/diesel-particulate-filters-r19

[18] T. Johnson, "Diesel Engine Emissions and Their Control," *Platinum Metals Review*, vol. 52, no. 1, pp. 23–37, Jan. 2008.

[19] S. Bremm, M. Pfeifer, J. Leyrer, W. Mueller, S. Kurze, M. Paule, B. Keppeler, and G. Vent, "Bluetec emission control system for the US tier 2 Bin 5 legislation," SAE Technical Paper, Tech. Rep., 2008.

[20] B. Guan, R. Zhan, H. Lin, and Z. Huang, "Review of state of the art technologies of selective catalytic reduction of NOx from diesel engine exhaust," *Applied Thermal Engineering*, vol. 66, no. 1–2, pp. 395–414, May 2014.

[21] K. Kamasamudram, A. Yezerets, X. chen, N. Currier, M. Castagnola, and H.-Y. Chen, "New Insights into Reaction Mechanism of Selective Catalytic Ammonia Oxidation Technology for Diesel Aftertreatment Applications," SAE International, Warrendale, PA, Tech. Rep. 2011-01-1314, Apr. 2011.

[22] A. König, W. Held, and T. Richter, "Lean-burn catalysts from the perspective of a car manufacturer. Early work at Volkswagen research," *Topics in catalysis*, vol. 28, no. 1-4, pp. 99–103, 2004.

[23] I. Nova and E. Tronconi, Eds., *Urea-SCR Technology for deNOx After Treatment of Diesel Exhausts*, ser. Fundamental and Applied Catalysis. New York, NY: Springer New York, 2014.

[24] R. Finesso, D. Misul, and E. Spessa, "Estimation of the Engine-Out NO2/NOx Ratio in a EURO VI Diesel Engine," SAE International, Warrendale, PA, SAE Technical Paper 2013-01-0317, Apr. 2013.

[25] J. W. Girard, C. Montreuil, J. Kim, G. Cavataio, and C. Lambert, "Technical Advantages of Vanadium SCR Systems for Diesel NOx Control in Emerging Markets," SAE International, Warrendale, PA, SAE Technical Paper 2008-01-1029, Apr. 2008.

[26] "Honeycomb Ceramics." [Online]. Available: http://sqsx-tech.en.frbiz.com/images/p40654864-honeycomb_ceramics.html

[27] A. Majewski, "Urea Dosing and Injection Systems," 2014. [Online]. Available: https://www.dieselnet.com/tech/cat_scr_mobile_urea_dosing.php

[28] "Bosch-Automotive," Oct. 2015. [Online]. Available: http://www.bosch-automotive.com

[29] B. K. Yun and M. Y. Kim, "Modeling the selective catalytic reduction of NOx by ammonia over a Vanadia-based catalyst from heavy duty diesel exhaust gases," *Applied Thermal Engineering*, vol. 50, no. 1, pp. 152–158, Jan. 2013.

[30] K. Kamasamudram, N. W. Currier, X. Chen, and A. Yezerets, "Overview of the practically important behaviors of zeolite-based urea-SCR catalysts, using compact experimental protocol," *Catalysis Today*, vol. 151, no. 3-4, pp. 212–222, Jun. 2010.

[31] Z. Skaf, T. Aliyev, L. Shead, and T. Steffen, "The State of the Art in Selective Catalytic Reduction Control," Apr. 2014.

[32] Q. Song and G. Zhu, "Model-based closed-loop control of urea SCR exhaust aftertreatment system for diesel engine," SAE Technical Paper, Tech. Rep., 2002.

[33] F. Willems, E. Van den Eijnden, M. van Genderen, and R. Verbeek, "Is Closed-Loop SCR Control Required to Meet Future Emission Targets?" SAE International, Tech. Rep., 2007.

[34] A. Herman, M.-C. Wu, D. Cabush, and M. Shost, "Model based control of scr dosing and obd strategies with feedback from nh3 sensors," *SAE Int. J. Fuels Lubr.*, vol. 2, pp. 375–385, 2009.

[35] D. Y. Wang, S. Yao, M. Shost, J.-H. Yoo, D. Cabush, D. Racine, R. Cloudt, and F. Willems, "Ammonia sensor for closed-Loop SCR control," SAE Technical Paper, Tech. Rep., 2008.

[36] M.-F. Hsieh and J. Wang, "Adaptive and efficient ammonia storage distribution control for a two-catalyst selective catalytic reduction system," *Journal of Dynamic Systems, Measurement, and Control*, vol. 134, no. 1, p. 011012, 2012.

[37] T. L. McKinley and A. G. Alleyne, "Model Predictive Control: A Unified Approach for Urea-Based SCR Systems," SAE Technical Paper, Tech. Rep., 2010.

[38] S. Stadlbauer, H. Waschl, and L. d. Re, "Adaptive SCR Model for MPC Control Including Aging Effects," SAE International, Warrendale, PA, SAE Technical Paper 2015-01-1045, Apr. 2015.

[39] M. Naseri, S. Chatterjee, M. Castagnola, H.-Y. Chen, J. Fedeyko, H. Hess, and J. Li, "Development of SCR on Diesel Particulate Filter System for Heavy Duty Applications," Apr. 2011.

[40] G. Cavataio, J. Y. Kim, J. R. Warner, J. W. Girard, D. Upadhyay, and C. K. Lambert, "Development of Emission Transfer Functions for Predicting the Deterioration of a Cu-Zeolite SCR Catalyst," SAE International, Warrendale, PA, SAE Technical Paper 2009-01-1282, Apr. 2009.

[41] X. Song, J. H. Johnson, and J. D. Naber, "A review of the literature of selective catalytic reduction catalysts integrated into diesel particulate filters," *International Journal of Engine Research*, Aug. 2014.

[42] T. C. Watling, M. R. Ravenscroft, and G. Avery, "Development, validation and application of a model for an SCR catalyst coated diesel particulate filter," *Catalysis Today*, vol. 188, no. 1, pp. 32–41, Jul. 2012.

[43] F. Schrade, M. Brammer, J. Schaeffner, K. Langeheinecke, and L. Kraemer, "Physico-Chemical Modeling of an Integrated SCR on DPF (SCR/DPF) System," SAE International, Warrendale, PA, Tech. Rep. 2012-01-1083, Apr. 2012.

[44] K. Rappé, "Integrated selective catalytic reduction-diesel particulate filter aftertreatment: Insights into pressure drop, NOx conversion, and passive soot oxidation behavior," *Industrial and Engineering Chemistry Research*, vol. 53, no. 45, pp. 17 547–17 557, 2014.

[45] J. Tan, C. Solbrig, and S. J. Schmieg, "The Development of Advanced 2-Way SCR/DPF Systems to Meet Future Heavy-Duty Diesel Emissions," SAE International, Warrendale, PA, SAE Technical Paper 2011-01-1140, Apr. 2011.

[46] J. Figura, D. Kihas, J. Pekar, M. Uchanski, N. Khaled, and S. Srinivasan, "Automotive Selective Catalytic Reduction System Model-based Estimators for on-ECU Implementation: A Brief Overview," submitted to SAE 2016 World Congress and Exhibition, SAE Technical Paper 2016-01-XXXX, 2016.

[47] X. Song, J. D. Naber, and J. H. Johnson, "A study of the effects of NH3 maldistribution on a urea-selective catalytic reduction system," *International Journal of Engine Research*, vol. 16, no. 2, pp. 213–222, Feb. 2015.

[48] M. K. Sampath and F. Lacin, "CFD Study of Sensitivity Parameters in SCR NOx Reduction Modeling," SAE International, Warrendale, PA, SAE Technical Paper 2014-01-2346, Sep. 2014.

[49] C.-T. Chen and W.-L. Tan, "Mathematical modeling, optimal design and control of an SCR reactor for NOx removal," *Journal of the Taiwan Institute of Chemical Engineers*, vol. 43, no. 3, pp. 409–419, May 2012.

[50] B. Hollauf, B. Breitsch, T. Sacher, M. Sch, and others, "Highest NOx Conversion in SCR Catalysts through Model Based Control," SAE Technical Paper, Tech. Rep., 2011.

[51] D. Upadhyay and M. Van Nieuwstadt, "Modeling of a Urea SCR Catalyst With Automotive Applications," pp. 707–713, Jan. 2002.

[52] C. Ericson, B. Westerberg, and I. Odenbrand, "A state-space simplified SCR catalyst model for real time applications," SAE Technical Paper, Tech. Rep., 2008.

[53] H. Na, D. Reed, A. Annaswamy, P. M. Laing, and I. Kolmanovsky, "Control-oriented Reduced-order Models for Urea Selective Catalytic Reduction Systems Using a Physics-based Approach," SAE International, Warrendale, PA, Tech. Rep. 2011-01-1326, Apr. 2011.

[54] M. Shost, J. Noetzel, M.-C. Wu, T. Sugiarto, T. Bordewyk, G. Fulks, and G. B. Fisher, "Monitoring, Feedback and Control of Urea SCR Dosing Systems for NOx Reduction: Utilizing an Embedded Model and Ammonia Sensing," SAE Technical Paper, Tech. Rep., 2008.

[55] X. Song, G. Parker, J. H. Johnson, J. Naber, and J. Pihl, "A Modeling Study of SCR Reaction Kinetics from Reactor Experiments," SAE International, Warrendale, PA, Tech. Rep. 2013-01-1576, Apr. 2013.

[56] M.-F. Hsieh and J. Wang, "Development and experimental studies of a control-oriented SCR model for a two-catalyst urea-SCR system," *Control Engineering Practice*, vol. 19, no. 4, pp. 409–422, Apr. 2011.

[57] M. F. Hsieh and J. Wang, "Nonlinear observer designs for diesel engine selective catalytic reduction (SCR) ammonia coverage ratio estimation," in *Proceedings of the 48th IEEE Conference on Decision and Control, 2009 held jointly with the 2009 28th Chinese Control Conference. CDC/CCC 2009*, Dec. 2009, pp. 6596–6601.

[58] H. S. Surenahalli, G. Parker, and J. H. Johnson, "Extended Kalman Filter Estimator for NH3 Storage, NO, NO2 and NH3 Estimation in a SCR," SAE International, Warrendale, PA, Tech. Rep. 2013-01-1581, Apr. 2013.

[59] M. F. Hsieh and J. Wang, "Sliding-mode observer for urea-selective catalytic reduction (SCR) mid-catalyst ammonia concentration estimation," *International Journal of Automotive Technology*, vol. 2, no. 3, pp. 321–329, 2011.

[60] H. Zhang, J. Wang, and Y.-Y. Wang, "Nonlinear Observer Design of Diesel Engine Selective Catalytic Reduction Systems With NOx Sensor Measurements," *IEEE/ASME Transactions on Mechatronics*, pp. 01–10, 2014.

[61] C. M. Schär, "Control of a selective catalytic reduction process," Ph.D. dissertation, IMRT Press c/o Institut für Mess- und Regeltechnik, ETH Zentrum, 2003.

[62] M. Devarakonda, G. Parker, J. H. Johnson, V. Strots, and S. Santhanam, "Model-based estimation and control system development in a urea-SCR aftertreatment system," SAE Technical Paper, Tech. Rep., 2008.

[63] X. Song, J. Naber, J. H. Johnson, and G. Parker, "An Experimental and Modeling Study of Reaction Kinetics for a Cu-Zeolite SCR Catalyst Based on Engine Experiments," SAE International, Warrendale, PA, SAE Technical Paper 2013-01-1054, Apr. 2013.

[64] T. L. McKinley, "Adaptive model predictive control of diesel engine selective catalytic reduction (SCR) systems," Ph.D. dissertation, 2009. [Online]. Available: https://www.ideals.illinois.edu/handle/2142/45106

[65] H. Zhang, J. Wang, and Y.-Y. Wang, "Removal of NOx sensor ammonia cross sensitivity from contaminated measurements in Diesel-engine selective catalytic reduction systems," *Fuel*, vol. 150, pp. 448–456, Jun. 2015.

[66] H. Zhang, J. Wang, and Y. Wang, "Robust Filtering for Ammonia Coverage Estimation in Diesel Engine Selective Catalytic Reduction Systems," *Journal of Dynamic Systems, Measurement, and Control*, vol. 135, no. 6, pp. 064 504–064 504, Aug. 2013.

[67] M. Meisami-Azad, J. Mohammadpour, K. Grigoriadis, M. Harold, and M. Franchek, "PCA-based linear parameter varying control of SCR aftertreatment systems," in *American Control Conference (ACC), 2011*, Jun. 2011, pp. 1543–1548.

[68] P. Chen and J. Wang, "A novel cost-effective robust approach for selective catalytic reduction state estimations using dual nitrogen oxide sensors," *Proceedings of the Institution of Mechanical Engineers, Part D: Journal of Automobile Engineering*, vol. 229, no. 1, pp. 83–96, Jan. 2015.

[69] P. Chen and J. Wang, "Sliding-mode observers for urea selective catalytic reduction system state estimations based on nitrogen oxide sensor measurements," *Proceedings of the Institution of Mechanical Engineers, Part D: Journal of Automobile Engineering*, vol. 229, no. 7, pp. 835–849, Jun. 2015.

[70] D. Upadhyay and M. Van Nieuwstadt, "Model Based Analysis and Control Design of a Urea-SCR deNOx Aftertreatment System," *Journal of Dynamic Systems, Measurement, and Control*, vol. 128, no. 3, p. 737, 2006.

[71] M. F. Hsieh and J. Wang, "An extended Kalman filter for NOx sensor ammonia cross-sensitivity elimination in selective catalytic reduction applications," in *American Control Conference (ACC), 2010*. IEEE, 2010, pp. 3033–3038.

[72] G. Zhou, J. B. Jørgensen, C. Duwig, and J. K. Huusom, "State estimation in the automotive SCR deNOx process," in *Proceedings of 8th IFAC Symposium on Advanced Control of Chemical Processes*, 2012, pp. 501–506.

[73] M.-F. Hsieh and J. Wang, "Design and experimental validation of an extended Kalman filter-based NOx concentration estimator in selective catalytic reduction system applications," *Control Engineering Practice*, vol. 19, no. 4, pp. 346–353, Apr. 2011.

[74] P. J. McCarthy, C. Nielsen, and S. L. Smith, "A nonlinear switched observer with projected state estimates for diesel engine emissions reduction," in *American Control Conference (ACC), 2013*. IEEE, 2013, pp. 1063–1068.

[75] H. Zhang, J. Wang, and Y.-Y. Wang, "Sensor Reduction in Diesel Engine Two-Cell Selective Catalytic Reduction (SCR) Systems for Automotive Applications," *IEEE/ASME Transactions on Mechatronics*, pp. 1–12, 2014.

[76] P. Chen and J. Wang, "Estimation of automotive urea-based selective catalytic reduction systems during low temperature operations," in *American Control Conference (ACC), 2014*, Jun. 2014, pp. 1523–1528.

[77] H. Zhang and J. Wang, "Ammonia coverage ratio and input simultaneous estimation in ground vehicle selective catalytic reduction (SCR) systems," *Journal of the Franklin Institute*, vol. 352, no. 2, pp. 708–723, Feb. 2015.

[78] H. Zhang and J. Wang, "NOx Sensor Ammonia-Cross-Sensitivity Factor Estimation in Diesel Engine Selective Catalytic Reduction Systems," *Journal of Dynamic Systems, Measurement, and Control*, vol. 137, no. 6, p. 061015, 2015.

[79] Y.-Y. Wang, H. Zhang, and J. Wang, "NOx Sensor Reading Correction in Diesel Engine Selective Catalytic Reduction System Applications," *IEEE/ASME Transactions on Mechatronics*, pp. 1–1, 2015.

[80] F. Willems and R. Cloudt, "Experimental Demonstration of a New Model-Based SCR Control Strategy for Cleaner Heavy-Duty Diesel Engines," *IEEE Transactions on Control Systems Technology*, vol. 19, no. 5, pp. 1305–1313, Sep. 2011.

[81] M. F. Hsieh and J. Wang, "Diesel Engine Selective Catalytic Reduction (SCR) Ammonia Surface Coverage Control Using a Computationally-Efficient Model Predictive Control Assisted Method," in *ASME 2009 Dynamic Systems and Control Conference*. American Society of Mechanical Engineers, 2009, pp. 865–872.

[82] A. Bonfils, Y. Creff, O. Lepreux, and N. Petit, "Closed-loop control of a SCR system using a NOx sensor cross-sensitive to NH3," *Journal of Process Control*, vol. 24, no. 2, pp. 368–378, Feb. 2014.

[83] P. Chavannavar, "Development and Implementation of a Mapless, Model Based SCR Control System," *SAE International Journal of Engines*, vol. 7, no. 2, pp. 1113–1124, Jul. 2014.

[84] T. L. McKinley and A. G. Alleyne, "Adaptive Model Predictive Control of an SCR Catalytic Converter System for Automotive Applications," *IEEE Transactions on Control Systems Technology*, vol. 20, no. 6, pp. 1533–1547, Nov. 2012.

[85] P. Chen and J. Wang, "Nonlinear Model Predictive Control of Integrated Diesel Engine and SCR System for Simultaneous Fuel Economy Improvement and Emissions Reduction," 2015.

[86] J. Balland, M. Parmentier, and J. Schmitt, "Control of a Combined SCR on Filter and Under-Floor SCR System for Low Emission Passenger Cars," *SAE International Journal of Engines*, vol. 7, no. 3, pp. 1252–1261, Apr. 2014.

[87] J. Figura, J. Tabacek, J. Tomasek, and D. Vojna, “Simplified Fast SCR Reaction Model with Ammonia Observer and MPC Control,” FEE, Czech Technical University in Prague, Final report for A3M99PTO, 2015.

[88] C. Depcik and D. Assanis, “One-dimensional automotive catalyst modeling,” *Progress in Energy and Combustion Science*, vol. 31, no. 4, pp. 308–369, Jan. 2005. [Online]. Available: http://linkinghub.elsevier.com/retrieve/pii/S0360128505000237

[89] R. Fazio and A. Jannelli, “Second order positive schemes by means of flux limiters for the advection equation,” *IAENG Int. J. Appl. Math*, vol. 39, no. 1, pp. 25–35, 2009. [Online]. Available: http://www.ewp.rpi.edu/hartford/~ernesto/Su2011/EP/MaterialsforStudents/Ferrari/Fazio2009.PDF

[90] D. S. Balsara, “Numerical PDE Techniques for Scientists and Engineers,” 2013. [Online]. Available: http://www3.nd.edu/~dbalsara/Numerical-PDE-Course/index.shtml

[91] M. Tutuianu, P. Bonnel, B. Ciuffo, T. Haniu, N. Ichikawa, A. Marotta, J. Pavlovic, and H. Steven, “Development of the World-wide harmonized Light duty Test Cycle (WLTC) and a possible pathway for its introduction in the European legislation,” *Transportation Research Part D: Transport and Environment*, vol. 40, pp. 61–75, Oct. 2015.

[92] M. S. Grewal and A. P. Andrews, *Kalman filtering theory and practice using MATLAB*. New York: Wiley, 2001.

[93] D. Simon, *Optimal state estimation: Kalman, H [infinity], and nonlinear approaches*. Hoboken, NJ: Wiley-Interscience, 2006.

[94] G. Bierman, “Measurement updating using the U-D factorization,” in *1975 IEEE Conference on Decision and Control including the 14th Symposium on Adaptive Processes*, Dec. 1975, pp. 337–346.

[95] C. Thornton and G. Bierman, “Gram-Schmidt algorithms for covariance propagation,” in *1975 IEEE Conference on Decision and Control including the 14th Symposium on Adaptive Processes*, Dec. 1975, pp. 489–498.

[96] V. M. Becerra, P. D. Roberts, and G. W. Griffiths, “Applying the extended Kalman filter to systems described by nonlinear differential-algebraic equations,” *Control Engineering Practice*, vol. 9, no. 3, pp. 267–281, 2001.